Postprint of: Kumar Jena S., Chakraverty S., Malikan M., Sedighi H.M.: Implementation of Hermite-Ritz method and Navier's Technique for Vibration of Functionally Graded Porous Nanobeam Embedded in Winkler-Pasternak Elastic Foundation Using bi-Helmholtz type of nonlocal elasticity. JOURNAL OF MECHANICS OF MATERIALS AND STRUCTURES. (2020). https://doi.org/10.2140/jomms.2020.15.405

Implementation of Hermite-Ritz method and Navier's Technique for Vibration of Functionally Graded Porous Nanobeam Embedded in Winkler-Pasternak Elastic Foundation Using bi-Helmholtz type of nonlocal elasticity

Subrat Kumar Jena[1], S. Chakraverty[2]*, Mohammad Malikan[3], Hamid Mohammad Sedighi[4,5]

[1, 2]Department of Mathematics, National Institute of Technology Rourkela, 769008, India

[3]Department of Mechanics of Materials and Structures, Faculty of Civil and Environmental Engineering, Gdansk University of Technology, Gdansk, P.O. Box 80-233, Poland

[4]Mechanical Engineering Department, Shahid Chamran University of Ahvaz, Ahvaz, P.O. Box 61357-43337, Iran

[5]Drilling Center of Excellence and Research Center, Shahid Chamran University of Ahvaz, Ahvaz, Iran

*Corresponding author

E-mail: [1]sjena430@gmail.com, [2]sne_chak@yahoo.com, [3]mohammad.malikan@pg.edu.pl, [4]h.msedighi@scu.ac.ir

Abstract

Present study is devoted to investigating the vibration characteristics of Functionally Graded (FG) porous nanobeam embedded in an elastic substrate of Winkler-Pasternak type. Classical beam theory (CBT) or Euler-Bernoulli beam theory (EBT) has been incorporated to address the displacement of the FG nanobeam. Bi-Helmholtz type of nonlocal elasticity is being used to

capture the small scale effect of the FG nanobeam. Further, the nanobeam is assumed to have porosity, distributed evenly along the thickness throughout the cross-section. Young's modulus and mass density of the nanobeam are considered to vary along the thickness from ceramic to metal constituents in accordance with power-law exponent model. A numerically efficient method, namely the Hermite-Ritz method, is incorporated to compute the natural frequencies of Hinged-Hinged (HH), Clamped-Hinged (CH), and Clamped-Clamped (CC) boundary conditions. A closed-form solution is also obtained for Hinged-Hinged (HH) boundary condition by employing Navier's technique. The advantages of using Hermite polynomials as shape functions are orthogonality, a large domain that makes the method more computationally efficient and avoids ill-conditioning for higher values of polynomials. Additionally, the present results are validated with other existing results in special cases demonstrating excellent agreement. A comprehensive study has been carried out to justify the effectiveness or convergence of the present model or method. Likewise, impacts of various scaling parameters such as Helmholtz and bi-Helmholtz types of nonlocal elasticity, porosity volume fraction index, power-law exponent, and elastic foundation on frequency parameters have been investigated.

Keywords

FG nanobeam; Hermite-Ritz method; Bi-Helmholtz function; Porosity; Winkler-Pasternak elastic foundation; vibration.

1. Introduction

Functionally graded materials (FGMs) are inhomogeneous materials consisting of two or more different materials, and the composition or volume of constituents varies continuously along one or more specific dimensions. As a result, their properties and structure will change steadily along the same dimension. This idea was first used by Japanese researchers [Koizumi 1994]. The gradual and continuous changes in these materials have made them very important and useful properties for application in various industries.

The introduction of FGMs to nano-micro technology has led to the development of devices and tools with better properties and capabilities, such as nano-micro-electro-mechanical systems (NEMS/MEMS), thin shape memory alloys, and atomic light microscopy. Nanotechnology is the study of microscopic objects about 1 to 100 nanometers in size and their applicability in various fields of science, such as chemistry, biology, physics, materials science, and engineering.

Recently, due to the special mechanical properties of nanostructures, the application of these structures has been developed in engineering, and researchers have been designing high-performance tools such as nanosensors, nano actuators, nanogenerators, etc. to solve new problems. Nanoscale tools are designed using the properties of nanotubes, nanobeams, nano-membranes, and nanosheets, so the discussion of modeling and analysis of nanobeams has attracted the attention of researchers.

Many experiments and computer simulations (molecular simulation) proved that a nanostructure mechanically has different response while it is analyzed in nanoscale size compared with a macroscale investigation. They showed that size is a crucial factor on nanoscale. Among all tools which aid us to predict mechanical response of these materials, the non-classical continuum elasticity approaches are cost and time-effective methods. Accordingly, it has been observed that classical continuum theories do not provide the right answer in predicting the behavior of these small scale structures. In fact, classical continuum theory is unable to account for size effects. The most popular non-classical continuum mechanic theories are: strain gradient theory [Mindlin 1965], nonlocal elasticity theory [Eringen 2002; Jena et al. 2019a; 2020a; 2020b], stress-driven nonlocal elasticity theory [Barretta et al. 2018; Sedighi and Malikan 2020], nonlocal strain gradient theory [Lim et al. 2015; Jena et al. 2019b; Malikan et al. 2020], modified coupled stress theory [Malikan 2017], surface elasticity theory [Ansari et al. 2013], and bi-Helmholtz nonlocal elasticity theory [Lazar et al. 2006; Koutsoumaris and Eptaimeros 2018]. These aforesaid theories, each in turn has small scale parameters. The small scale parameter makes difference between macro scale and nanoscale. Many research approved that these scale parameters are not material constant and vary with variation in natural features and physical characteristics of the nanomaterial. As an example, boundary and edge conditions affect fundamentally the values of small scale parameter. Moreover, as the nano materials except for being size-dependent, are also temperature-dependent, the thermal environment can significantly affect the value of small scale parameter. Thus, a nanostructure in various boundary conditions and different external temperature requires different values for the small scale parameter to give exact results. That is why all the researchers presented amplitude for numerical values of small scale parameters. There are also further examples for factors that affect the amount of a small scale parameter, such as crack specifications in cracked nanomaterials, arrangement of atoms in atomic lattice into some special nanomaterials like graphene and nanotubes with changeable arrangement (chirality effect), etc.

The mechanical behavior of FG nanomaterials with different geometries and various loading and boundary conditions has been extensively investigated by researchers in the current decade. Beams are of great importance due to their wide use in engineering. To date, numerous articles have been written on the study of the dynamics of FGM nanobeams. Eltaher et al. [2012] based on the finite element method (FEM) analyzed natural frequencies of a nanoscale FGM beam by considering nonlocal continuum mechanics. The beam was modeled according to the Euler-Bernoulli beam theory (EBT) approach. The numerical outputs were calculated for a variety of boundary conditions. Sharabiania and Yazdi [2013] depicted a nonlinear frequency analysis on FGM nanosize beams in the framework of EBT while the size dependency was investigated on the basis of surface effects. The results were shown for some different edge conditions. Esmaeili and Tadi Beni [2019] investigated buckling and vibration characteristics of flexoelectric smart nanobeam composed of functionally graded materials. Nazemnezhad and Hosseini-Hashemi [2014] studied nonlocal effects within the framework of nonlinear analysis of vibrations for FGM nanoscale beams. The immovable ends, such as fixed and pinned conditions were assumed when EBT was employed to give the constitutive equations of frequency. Hashemi et al. [2014] considered analytically effects of surface and stress nonlocality for pivot-pivot EBT-FGM nanobeam models. Ansari et al. [2015] examined the excited frequencies nonlinearly for an FGM nanobeam in the body of an exact solution. The influences of the environment, such as temperature differential, were measured as well. The nanosize into the EBT model was investigated utilizing surface elasticity theory, and the Galerkin technique helped to solve the attained equations. Zeighampour and Tadi Beni [2015] developed FGM nanobeams by considering the variation of diameter in the length direction. The strain gradient theory, EBT, and Visco-Pasternak foundation model were combined, which led to the governing equations. The obtained equations were discretized using differential quadrature method (DQM) for pined-pined and clamped-clamped supported and then were solved by eigenvalue solver. Their best results proved the considerable effect of diameter variation on the dynamics behavior of FGM nanobeams. Ebrahimi and Salari [2015] studied the nonlocal effect on the FGM nanobeams by considering EBT beam model with the presence and absence of the influences of the thermal environment utilizing analytical method based on the Navier method.

Simsek [2016] discussed the free vibration of an FGM nanoscale beam based on the nonlinear strains and derived mathematical relation by presenting a new Hamiltonian in combining with EBT and nonlocal strain gradient elasticity. Shafiei et al. [2016] modeled a non-uniform FGM beam taking nanosize effects based on the nonlocal theory of elasticity. The natural frequencies were captured for the beam with the contribution of nonlinear terms. The procedure for solving of the harvested equations was generalized differential quadrature (GDQ) method and Homotopy perturbation method for fixed-fixed, pinned-pinned, and fixed-pinned boundary conditions. Hosseini and Rahmani [2016] combined thermos-elastic relations to study vibrations of an FGM nanoscale beam when the beam is geometrically curved. The nonlocal elasticity provides the size-dependent behavior, and the numerical results were obtained by analytical solutions. Khorshidi and Shariati [2016] investigated the vibration characteristics of the sigmoid-type of FGM nanobeams by using the modified couple stress theory. A variety of beam hypotheses such as EBT, first-order shear deformation theory (FSDT) and some higher-order shear deformation theory (HSDT) were investigated with the help of GDQ. Vosoughi [2016] applied nonlinearity to study free vibration of a FGM nanosize beam embedded on a nonlinear elastic medium. The use of FSDT and nonlocal elasticity addressed the desired equations that were discretized by DQM. Hamed et al. [2016] compared sigmoid with a nonlinear symmetric power varied along the thickness of EB-FGM nonlocal beams in a vibration study. Saffari et al. [2017] inspected the stability of an FGM nonlocal FSDT beam by taking surface effects in a dynamical situation. Thermal effects and foundation influences were implemented as well. Arefi and Zenkour [2017] explored the nonlocal vibration of a Timoshenko FGM nanobeam by taking the Visco-Pasternak matrix into account.

Vu-Bac et al. [2016] carried out sensitivity analysis for quantifying the influence of uncertain input parameters by using probability density function on uncertain model outputs. The dynamics of three-dimensional inhomogeneities of FGM nanoscale beams was investigated by Hadi et al. [2018]. Jouneghani et al. [2018] modeled porosity into the material gradation of FGM nanobeams and examined the structural behavior of the system subjected to variation of environmental parameters such as temperature and humidity. Mirjavadi et al. [2018] focused on the nonlinear behavior of FGM nanosize beams considering porosities with respect to the EBT and second stress gradient of Eringen. Different end conditions were taken into consideration by the assistance of GDQM and an iterative technique. Simsek [2019] performed different closed-form approaches to study a variety of analyses on the FGM nanobeams, namely forced and free vibrations, static bending, and buckling. The nonlocal strain gradient theory was implemented to capture the size dependency influence. Various loading cases were demonstrated in the dynamic analysis of the graded EBT model.

Aria and Friswell [2019] indicated a finite element analysis in the form of nonlocality to consider free vibration and stability of FGM nanobeams. Uzun and Yayli [2019] investigated the free vibration of functionally graded nanobeam for hinged-hinged and clamped-clamped boundary conditions with the help of the finite element model. The nonlocal effect of FG nanobeam was handled by the Eringen's nonlocal theory. Karami and Janghorban [2019] showed a new shaped function into the higher-order shear deformation theory to study analytically natural frequencies of a FGM nonlocal isotropic/anisotropic beam. Thickness stretching influence was also evaluated by the shape function. The nonlocal strain gradient model determined the nanoscale behavior. Khaniki [2019] studied vibrations of FGM nanoscale beams based on the two phases nonlocal-local models, and then functionality gradation was derived along length. GDQ helped to obtain numerical results. Chen et al. [2020] studied thermal buckling behavior of Euler-Bernoulli beam made up of FG material. The transformed-section method was used to investigate the buckling characteristics analytically. Uzun and Yayli [2020] in a pioneering work studied free vibration of functionally graded nanobeam for Simply Supported boundary condition using Euler-Bernoulli beam theory and Eringen's nonlocal elasticity by utilizing FEM.

Previous studies, as mentioned above illustrate the fact that the studies involving non-classical theories have rarely used the Bi-Helmholtz nonlocal elasticity theory; and have never used the advanced yet simple Hermit-Ritz method for this purpose. In this study, the Euler-Bernoulli theory is applied to find the numerical response of free vibration of FG nanobeams. The numerical solution of the free vibration is obtained, and the response of the rectangular nanobeam is calculated for the bi-Helmholtz nonlocal parameter by employing the Hermit-Ritz method for HH, CH, and CC boundary conditions while closed-form solution is obtained for HH boundary condition by utilizing the Navier's technique. The beam is also embedded on the Winkler-Pasternak elastic bed. Due to the importance of porosity in the structure of functionally graded materials, this argument is included in the present analysis as well. The results of the theory presented are compared with those reported by previous researchers, and a good agreement is observed between the results. A parametric analysis is also carried out to investigate the effect of various scaling parameters such as Helmholtz and bi-Helmholtz types of nonlocal elasticity, porosity volume fraction index, power-law exponent, and elastic foundation on the frequency response of the FG nanobeam.

2. Reviews of Helmholtz and bi-Helmholtz types of nonlocal operators

The bi- Helmholtz type nonlocal modulus, which is the Green's function of bi Helmholtz operator may be stated as [Lazar et al. 2006; Koutsoumaris and Eptaimeros 2018]

$$A^{bH}\left(|x-x'|\right)=\frac{1}{2}\frac{1}{\xi_1^2-\xi_2^2}\left\{\xi_1 e^{\frac{-|x-x'|}{\xi_1}}-\xi_2 e^{\frac{-|x-x'|}{\xi_2}}\right\} \tag{1}$$

The corresponding bi-Helmholtz operator may be expressed as [Eringen 2002; Lazar et al. 2006; Koutsoumaris and Eptaimeros 2018]

$$\ell^{bH}=\left(1-\xi_1^2\frac{d^2}{dx^2}\right)\left(1-\xi_2^2\frac{d^2}{dx^2}\right)=1-\left(\xi_1^2+\xi_2^2\right)\frac{d^2}{dx^2}+\xi_1^2\xi_2^2\frac{d^4}{dx^4}=1-\varepsilon^2\frac{d^2}{dx^2}+\gamma^4\frac{d^4}{dx^4}, \tag{2}$$

where $\varepsilon^2=\xi_1^2+\xi_2^2=(e_0 a)^2$, $\gamma^4=\xi_1^2\xi_2^2$ and the constants ξ_1 and ξ_2 are demonstrated as [Eringen 2002; Lazar et al. 2006; Koutsoumaris and Eptaimeros 2018]

$$\xi_1^2=\frac{\varepsilon^2}{2}\left(1+\sqrt{1-4\frac{\gamma^4}{\varepsilon^4}}\right) \tag{3.a}$$

$$\xi_2^2=\frac{\varepsilon^2}{2}\left(1-\sqrt{1-4\frac{\gamma^4}{\varepsilon^4}}\right) \tag{3.b}$$

Here the discriminant $\left(1-4\frac{\gamma^4}{\varepsilon^4}\right)\geq 0$, i.e., $\varepsilon\geq\sqrt{2}\gamma$. Considering $\varepsilon=\sqrt{2}\gamma$, we will have $\xi_1=\xi_2$, where $\xi_1,\xi_2\in R$ and the parameter γ triumphs over ε . For any other case, i.e., $\varepsilon>\sqrt{2}\gamma$, the effect of ε prevails over γ. From Lazar et al. [2006], Koutsoumaris and Eptaimeros [2018], it is evident that that ℓ^{bH} operator matched the Born Karman's model at the end of the Brillouin zone, when $\xi_1=\xi_2$. Now, the nonlocal modulus is given in Eq. (1) maybe stated as [Lazar et al. 2006; Koutsoumaris and Eptaimeros 2018]

$$A^{bH}\left(|x-x'|,\gamma\right)=\frac{1}{2}\frac{1}{2\gamma^{2}}\left(\gamma+|x-x'|\right)e^{\frac{-|x-x'|}{\gamma}} \tag{4}$$

Substituting $\varepsilon=\sqrt{2}\gamma$ or $e_0a=\sqrt{2}\gamma$, Eq. (4) can be expressed as [Lazar et al. 2006; Koutsoumaris and Eptaimeros 2018]

$$A^{bH}\left(|x-x'|,\frac{e_0a}{\sqrt{2}}\right)=\frac{1}{2(e_0a)^2}\left(\frac{e_0a}{\sqrt{2}}+|x-x'|\right)e^{-\frac{\sqrt{2}|x-x'|}{e_0a}} \tag{5}$$

Thus, the bi-Helmholtz operator in differential form may be given as [Lazar et al. 2006; Koutsoumaris and Eptaimeros 2018]

$$\ell^{bH}=1-(e_0a)^2\frac{d^2}{dx^2}+\frac{(e_0a)^4}{4}\frac{d^4}{dx^4} \tag{6}$$

Assuming $\xi_1=e_0a$ and $\xi_2=0$ in Eq. (1), the Helmholtz-type nonlocal modulus is given as [Eringen 2002; Koutsoumaris and Eptaimeros 2018]

$$A^{H}\left(|x-x'|,e_0a\right)=\frac{1}{2(e_0a)}e^{\frac{-|x-x'|}{e_0a}}, \tag{7}$$

and the corresponding Helmholtz operator in differential form is given as [Eringen 2002]

$$\ell^{H}=1-(e_0a)^2\frac{d^2}{dx^2}. \tag{8}$$

3. Mathematical formulation of the proposed model

In this study, a functionally graded porous nanobeam with length (L), breadth (b), thickness (h), and porosity volume fraction $\vartheta, (\vartheta<1)$ is taken into consideration, as depicted in Fig. 1.a . The material composition at the top surface $(z=h/2)$ is assumed to be ceramic-rich while the bottom surface $(z=-h/2)$ is considered to be metal-rich, and the gradation along thickness from the ceramic-rich surface to metal-rich surface is governed by power-law variation model. The porosity in the nanobeam is assumed as evenly distributed throughout the metal and ceramic constituents, as illustrated in Fig. 1.b.

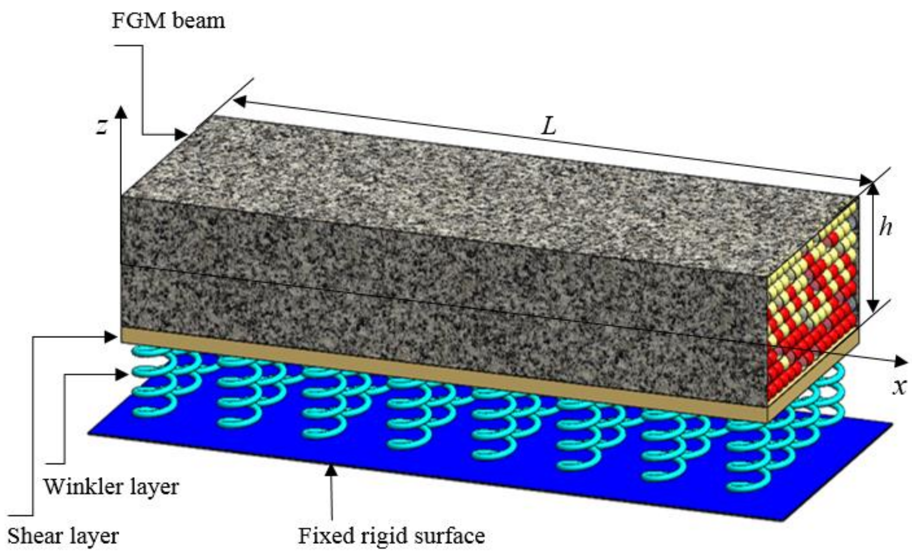

Fig 1.a Schematic diagram of rectangular FG nanobeam embedded in the Winkler-Pasternak elastic foundation.

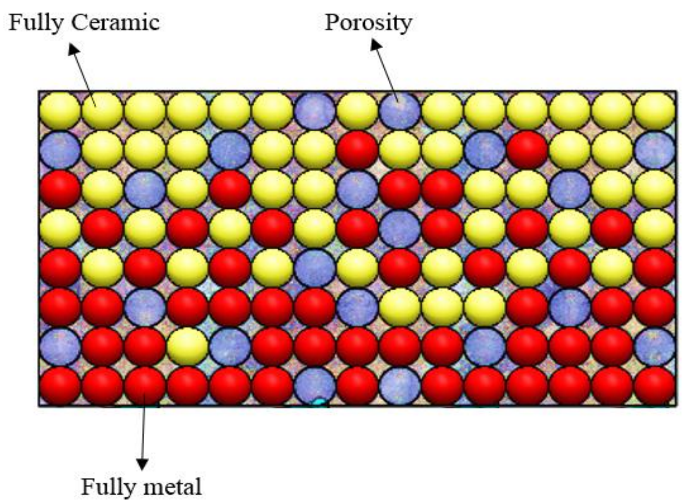

Fig 1.b Graphical representation of the rectangular cross-section of the FG nanobeam with evenly distributed porosity

Thus, according to the modified rule of the mixture [Wattanasakulpong and Ungbhakorn 2014; Shahsavari et al. 2018]

$$P = P_U V_U + P_L V_L - \frac{\vartheta}{2}\left(P_U + P_L\right) \tag{9}$$

Here P denotes the material property FG nanobeam. P_U , V_U is the material property and volume fraction for the ceramic constituent, whereas P_L , V_L symbolize the material property and volume fraction of the metal constituent.

As per the power law variation model, the volume fractions of the ceramic and metal components are expressed as [Wattanasakulpong and Ungbhakorn 2014; Shahsavari et al. 2018]

$$V_U = \left(\frac{z}{h} + \frac{1}{2} \right)^k \tag{10}$$

$$V_L = 1 - \left(\frac{z}{h} + \frac{1}{2} \right)^k \tag{11}$$

Where k is the non-negative parameter, namely power-law exponent, that regulates the distribution of material along the thickness of the nanobeam and z denotes the distance from the mid-plane of the FG nanobeam. Using Eq. (9), Eq. (10), and Eq. (11), the material properties of the FG nanobeam with porosity may be given as [Wattanasakulpong and Ungbhakorn 2014; Shahsavari et al. 2018]

$$P = (P_U - P_L)\left(\frac{z}{h} + \frac{1}{2} \right)^k + P_L - \frac{\vartheta}{2}(P_U + P_L) \tag{12}$$

The Young's modulus $E(z)$, and material density $\rho(z)$ of the FG nanobeam can be demonstrated graphically in Figs. (2-3) and mathematically as [Wattanasakulpong and Ungbhakorn 2014; Shahsavari et al. 2018]

$$E(z) = (E_U - E_L)\left(\frac{z}{h} + \frac{1}{2} \right)^k + E_L - \frac{\vartheta}{2}(E_U + E_L) \tag{13.a}$$

$$\rho(z) = (\rho_U - \rho_L)\left(\frac{z}{h} + \frac{1}{2} \right)^k + \rho_L - \frac{\vartheta}{2}(\rho_U + \rho_L) \tag{13.b}$$

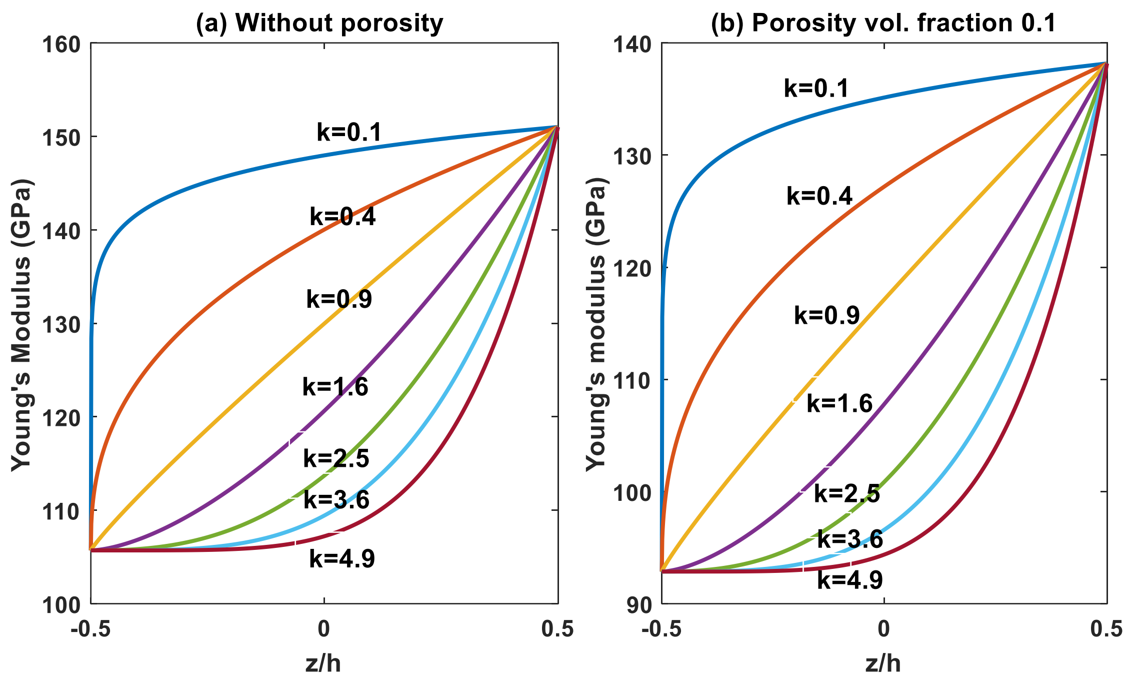

Fig. 2 Power-law variation of Young's modulus for FG nanabeam composed of alpha-beta titanium alloy (Ti-6AL-4V) and zirconia (ZrO_2)

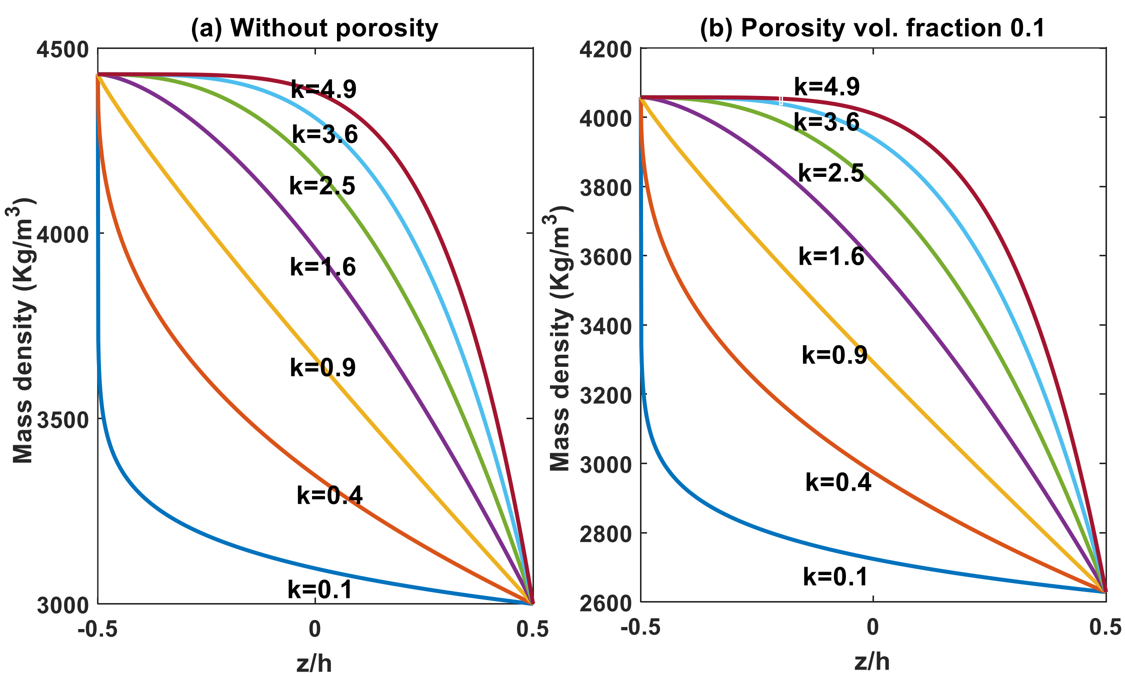

Fig. 3 Power-law variation of Mass density for FG nanabeam composed of alpha-beta titanium alloy (Ti-6AL-4V) and zirconia (ZrO_2)

According to the classical beam theory or Euler-Bernoulli beam theory, the displacement field can be given as [Reddy 2007]

$$u_1(x,z,t) = u(x,t) - z\left(\frac{\partial w}{\partial x}\right) \tag{14.a}$$

$$u_2(x,z,t) = 0 \tag{14.b}$$

$$u_3(x,z,t) = w(x,t) \tag{14.c}$$

Where $u(x,t)$, and $w(x,t)$ represent the axial and transverse displacements on the mid-plane of the FG nanobeam, respectively.

The strain-displacement relation of the FG nanobeam is stated as

$$\varepsilon_{xx} = \frac{\partial u_1(x,z,t)}{\partial x} = \frac{\partial u(x,t)}{\partial x} - z\frac{\partial^2 w(x,t)}{\partial x^2} \tag{15}$$

The stress component of the FG nanobeam as generalized Hooke's law may be given as [Pradhan and Chakraverty 2014]

$$\sigma_{xx} = Q_{11}\varepsilon_{xx} = \left(\frac{E(z)}{1-\upsilon^2}\right)\varepsilon_{xx} \tag{16}$$

3.1 Energy form of Equation for Hermite-Ritz method

The strain energy (S) of the FG nanobeam is stated as

$$\begin{aligned} S &= \frac{1}{2}\int_0^L \int_A (\sigma_{xx}\varepsilon_{xx})\,dA\,dx \\ &= \frac{1}{2}\int_0^L \int_A \left[\sigma_{xx}\left(\frac{\partial u(x,t)}{\partial x} - z\frac{\partial^2 w(x,t)}{\partial x^2}\right)\right] dA\,dx \\ &= \frac{1}{2}\int_0^L \left[N\left(\frac{\partial u(x,t)}{\partial x}\right) - M\left(\frac{\partial^2 w(x,t)}{\partial x^2}\right)\right] dx \end{aligned} \tag{17}$$

Where the stress resultants $(N, M) = \int_A (\sigma_{xx}, z\sigma_{xx})\,dA.$

Now, the variation in strain energy (δS) can be given as

$$
\begin{aligned}
\delta S &= \int_0^L \int_A \left(\sigma_{xx}\delta\varepsilon_{xx}\right) dA dx \\
&= \int_0^L \int_A \left[\sigma_{xx}\left(\frac{\partial \delta u(x,t)}{\partial x} - z\frac{\partial^2 \delta w(x,t)}{\partial x^2}\right)\right] dA dx \\
&= \int_0^L \left[N\left(\frac{\partial \delta u(x,t)}{\partial x}\right) - M\left(\frac{\partial^2 \delta w(x,t)}{\partial x^2}\right)\right] dx \\
&= \int_0^L \left[-\left(\frac{\partial N}{\partial x}\right)\delta u - \left(\frac{\partial^2 M}{\partial x^2}\right)\delta w\right] dx
\end{aligned}
\tag{18}
$$

The kinetic energy (T) of the FG nanobeam can be stated as

$$
\begin{aligned}
T &= \frac{1}{2}\int_0^L \int_A \rho(z)\left[\left(\frac{\partial u_1}{\partial t}\right)^2 + \left(\frac{\partial u_2}{\partial t}\right)^2 + \left(\frac{\partial u_3}{\partial t}\right)^2\right] dA dx \\
&= \frac{1}{2}\int_0^L \int_A \rho(z)\left[\left(\frac{\partial u}{\partial t} - z\left(\frac{\partial^2 w}{\partial x \partial t}\right)\right)^2 + \left(\frac{\partial w}{\partial t}\right)^2\right] dA dx \\
&= \frac{1}{2}\int_0^L \left[I_0\left(\left(\frac{\partial u}{\partial t}\right)^2 + \left(\frac{\partial w}{\partial t}\right)^2\right) - 2I_1\left(\frac{\partial u}{\partial t}\right)\left(\frac{\partial^2 w_b}{\partial x \partial t}\right) + I_2\left(\frac{\partial^2 w}{\partial x \partial t}\right)^2\right] dx
\end{aligned}
\tag{19}
$$

In which $(I_0, I_1, I_2) = \int_A \rho(z)(1, z, z^2) dA$ are the mass moment of inertias.

The variation in kinetic energy (δT) can be obtained from Eq. (19) as

$$
\begin{aligned}
\delta T &= \frac{1}{2}\int_0^L \left[I_0\delta\left(\left(\frac{\partial u}{\partial t}\right)^2 + \left(\frac{\partial w}{\partial t}\right)^2\right) - 2I_1\delta\left(\frac{\partial u}{\partial t}\right)\left(\frac{\partial^2 w_b}{\partial x \partial t}\right) + I_2\delta\left(\frac{\partial^2 w}{\partial x \partial t}\right)^2\right] dx \\
&= \int_0^L \left[-I_0\left(\frac{\partial^2 u}{\partial t^2}\right)\delta u - I_0\left(\frac{\partial^2 w}{\partial t^2}\right)\delta w + I_1\left(\frac{\partial^3 w}{\partial x \partial t^2}\right)\delta u - I_1\left(\frac{\partial^3 u}{\partial x \partial t^2}\right)\delta w + I_2\left(\frac{\partial^4 w}{\partial x^2 \partial t^2}\right)\delta w\right] dx
\end{aligned}
\tag{20}
$$

The work done (W) by the Winkler-Pasternak elastic foundation can be expressed as [Uzun and Yayl□ 2020]

$$
W = -\frac{1}{2}\int_0^L \left[k_w w^2 + k_g\left(\frac{\partial w}{\partial x}\right)^2\right] dx, \tag{21}
$$

where k_w and k_g are Winkler and Pasternak elastic constants, respectively.

The variation in external work done (δW) can be derived from Eq. (21) as

$$\delta W = -\int_0^L \left[k_w w + k_g \left(\frac{\partial^2 w}{\partial x^2} \right) \right] \delta w dx \tag{22}$$

Using Eq. (18), Eq. (20), and Eq.(22) in the extended Hamilton's principle $\int_0^T (T - S + W) dt = 0$ and collecting the co-efficient of δu and δw, the governing equations of motion in terms of stress resultants and displacements can be obtained as

$$\frac{\partial N}{\partial x} = I_0 \left(\frac{\partial^2 u}{\partial t^2} \right) - I_1 \left(\frac{\partial^3 w}{\partial x \partial t^2} \right) \tag{23.a}$$

$$\frac{\partial^2 M}{\partial x^2} = I_0 \left(\frac{\partial^2 w}{\partial t^2} \right) + I_1 \left(\frac{\partial^3 u}{\partial x \partial t^2} \right) - I_2 \left(\frac{\partial^4 w}{\partial x^2 \partial t^2} \right) + k_w w - k_g \left(\frac{\partial^2 w}{\partial x^2} \right) \tag{23.b}$$

Multiplying Eq. (16) by dA and $z\,dA$ and integrating over the area of cross-section of the FG nanobeam, the local stress resultants can be written as

$$N = A_{11} \left(\frac{\partial u}{\partial x} \right) - B_{11} \left(\frac{\partial^2 w}{\partial x^2} \right) \tag{24.a}$$

$$M = B_{11} \left(\frac{\partial u}{\partial x} \right) - D_{11} \left(\frac{\partial^2 w}{\partial x^2} \right), \tag{24.b}$$

where $(A_{11}, B_{11}, D_{11}) = \int_A Q_{11} (1, z, z^2) dA$, are the stiffness coefficients of FG nanobeam.

Applying bi-Helmholtz operator to Eq. (24) and using Eq. (23), the nonlocal stress resultant resultants of the FG nanobeam can be obtained as

$$N = A_{11} \left(\frac{\partial u}{\partial x} \right) - B_{11} \left(\frac{\partial^2 w}{\partial x^2} \right) + (e_0 a)^2 \left[\begin{array}{l} \left\{ I_0 \left(\frac{\partial^3 u}{\partial x \partial t^2} \right) - I_1 \left(\frac{\partial^4 w}{\partial x^2 \partial t^2} \right) \right\} - \frac{(e_0 a)^2}{4} \\ \left\{ I_0 \left(\frac{\partial^5 u}{\partial x^3 \partial t^2} \right) - I_1 \left(\frac{\partial^6 w}{\partial x^4 \partial t^2} \right) \right\} \end{array} \right] \tag{25.a}$$

$$M = B_{11}\left(\frac{\partial u}{\partial x}\right) - D_{11}\left(\frac{\partial^2 w}{\partial x^2}\right) + (e_0 a)^2 \left[\begin{array}{l} \left\{ \begin{array}{c} I_0\left(\frac{\partial^2 w}{\partial t^2}\right) + I_1\left(\frac{\partial^3 u}{\partial x \partial t^2}\right) - I_2\left(\frac{\partial^4 w}{\partial x^2 \partial t^2}\right) \\ + k_w w - k_g\left(\frac{\partial^2 w}{\partial x^2}\right) \end{array} \right\} \\ -\frac{(e_0 a)^2}{4} \left\{ \begin{array}{l} I_0\left(\frac{\partial^4 w}{\partial x^2 \partial t^2}\right) + I_1\left(\frac{\partial^5 u}{\partial x^3 \partial t^2}\right) - \\ I_2\left(\frac{\partial^6 w}{\partial x^4 \partial t^2}\right) + k_w\left(\frac{\partial^2 w}{\partial x^2}\right) - k_g\left(\frac{\partial^4 w}{\partial x^4}\right) \end{array} \right\} \end{array} \right] \tag{25.b}$$

Substituting Eq. (25) in Eq. (17), the strain energy, kinetic energy, and work done by elastic foundation for the FG nanobeam can be depicted as

$$T = \frac{1}{2}\int_0^L \left[I_0\left(\left(\frac{\partial u}{\partial t}\right)^2 + \left(\frac{\partial w}{\partial t}\right)^2\right) - 2I_1\left(\frac{\partial u}{\partial t}\right)\left(\frac{\partial^2 w_b}{\partial x \partial t}\right) + I_2\left(\frac{\partial^2 w}{\partial x \partial t}\right)^2 \right] dx \tag{26}$$

$$W = -\frac{1}{2}\int_0^L \left[k_w w^2 + k_g\left(\frac{\partial w}{\partial x}\right)^2 \right] dx \tag{27}$$

$$S = \frac{1}{2}\int_0^L \left[\begin{array}{l} A_{11}\left(\frac{\partial u}{\partial x}\right)^2 - 2B_{11}\left(\frac{\partial u}{\partial x}\right)\left(\frac{\partial^2 w}{\partial x^2}\right) + D_{11}\left(\frac{\partial^2 w}{\partial x^2}\right)^2 + \\ (e_0 a)^2\left(\frac{\partial u}{\partial x}\right)\left\{ I_0\left(\frac{\partial^3 u}{\partial x \partial t^2}\right) - I_1\left(\frac{\partial^4 w}{\partial x^2 \partial t^2}\right) \right\} \\ -\frac{(e_0 a)^4}{4}\left(\frac{\partial u}{\partial x}\right)\left\{ I_0\left(\frac{\partial^5 u}{\partial x^3 \partial t^2}\right) - I_1\left(\frac{\partial^6 w}{\partial x^4 \partial t^2}\right) \right\} + (e_0 a)^2\left(\frac{\partial^2 w}{\partial x^2}\right) \\ \left\{ I_0\left(\frac{\partial^2 w}{\partial t^2}\right) + I_1\left(\frac{\partial^3 u}{\partial x \partial t^2}\right) - I_2\left(\frac{\partial^4 w}{\partial x^2 \partial t^2}\right) + k_w w - k_g\left(\frac{\partial^2 w}{\partial x^2}\right) \right\} \\ -\frac{(e_0 a)^4}{4}\left(\frac{\partial^2 w}{\partial x^2}\right) \left\{ \begin{array}{l} I_0\left(\frac{\partial^4 w}{\partial x^2 \partial t^2}\right) + I_1\left(\frac{\partial^5 u}{\partial x^3 \partial t^2}\right) - I_2\left(\frac{\partial^6 w}{\partial x^4 \partial t^2}\right) \\ + k_w\left(\frac{\partial^2 w}{\partial x^2}\right) - k_g\left(\frac{\partial^4 w}{\partial x^4}\right) \end{array} \right\} \end{array} \right] dx \tag{28}$$

Assuming the motion of the FG nanobeam as sinusoidal i.e., plugging $u(x,t) = U(x)\cos(\omega t)$ and $w(x,t) = W(x)\cos(\omega t)$, the maximum strain energy $(S_{\max})$, kinetic energy $(T_{\max})$, and work done by elastic foundation $(W_{\max})$ for the FG nanobeam can be obtained as

$$S_{\max} = \frac{1}{2}\int_0^L \left[\begin{array}{l} A_{11}\left(\frac{dU}{dx}\right)^2 - 2B_{11}\left(\frac{dU}{dx}\right)\left(\frac{d^2W}{dx^2}\right) + D_{11}\left(\frac{d^2W}{dx^2}\right)^2 - (\omega)^2 (e_0 a)^2 I_0 \left(\frac{dU}{dx}\right)^2 \\ + 2(\omega)^2 (e_0 a)^2 I_1 \left(\frac{dU}{dx}\right)\left(\frac{d^2W}{dx^2}\right) + (\omega)^2 \frac{(e_0 a)^4}{4} I_0 \left(\frac{dU}{dx}\right)\left(\frac{d^3W}{dx^3}\right) + (\omega)^2 \\ \frac{(e_0 a)^4}{4} I_1 \left(\frac{dU}{dx}\right)\left(\frac{d^4W}{dx^4}\right) + (\omega)^2 (e_0 a)^2 I_0 (W)\left(\frac{d^2W}{dx^2}\right) - (\omega)^2 (e_0 a)^2 I_2 \\ \left(\frac{d^2W}{dx^2}\right)^2 - (e_0 a)^2 k_w (W)\left(\frac{d^2W}{dx^2}\right) + (e_0 a)^2 k_g \left(\frac{d^2W}{dx^2}\right)^2 - (\omega)^2 \frac{(e_0 a)^4}{4} I_0 \\ \left(\frac{d^2W}{dx^2}\right)^2 - (\omega)^2 \frac{(e_0 a)^4}{4} I_1 \left(\frac{d^2W}{dx^2}\right)\left(\frac{d^3U}{dx^3}\right) + (\omega)^2 \frac{(e_0 a)^4}{4} I_2 \left(\frac{d^2W}{dx^2}\right)\left(\frac{d^4W}{dx^4}\right) \\ - \frac{(e_0 a)^4}{4} k_g \left(\frac{d^2W}{dx^2}\right)\left(\frac{d^4W}{dx^4}\right) + \frac{(e_0 a)^4}{4} k_w \left(\frac{d^2W}{dx^2}\right)^2 \end{array} \right] dx \qquad (29)$$

$$T_{\max} = \frac{\omega^2}{2}\int_0^L \left[I_0\left(U^2 + W^2\right) - 2I_1(U)\left(\frac{dW}{dx}\right) + I_2\left(\frac{dW}{dx}\right)^2 \right] dx \qquad (30)$$

$$W_{\max} = -\frac{1}{2}\int_0^L \left[k_w W^2 + k_g \left(\frac{dW}{dx}\right)^2 \right] dx \qquad (31)$$

Substituting Eqs. (29-31) into Lagrangian energy function $\Pi = S_{\max} - W_{\max} - T_{\max}$ and setting $\Pi = 0$, one may get

$$\int_0^L \left[\begin{array}{l} A_{11}\left(\frac{dU}{dx}\right)^2 - 2B_{11}\left(\frac{d^2W}{dx^2}\right)\left(\frac{dU}{dx}\right) + D_{11}\left(\frac{d^2W}{dx^2}\right)^2 - (e_0a)^2 k_w (W)\left(\frac{d^2W}{dx^2}\right) + (e_0a)^2 \\ k_g\left(\frac{d^2W}{dx^2}\right)^2 + \frac{(e_0a)^4}{4} k_w \left(\frac{d^2W}{dx^2}\right)^2 - \frac{(e_0a)^4}{4} k_g \left(\frac{d^2W}{dx^2}\right)\left(\frac{d^4W}{dx^4}\right) + k_w W^2 + k_g\left(\frac{dW}{dx}\right)^2 \end{array}\right] dx$$

$$= \omega^2 \int_0^L \left[\begin{array}{l} I_0\left(U^2 + W^2\right) - 2I_1(U)\left(\frac{dW}{dx}\right) + I_2\left(\frac{dW}{dx}\right)^2 + (e_0a)^2 I_0\left(\frac{dU}{dx}\right)^2 - (e_0a)^2 I_1 \\ \left(\frac{dU}{dx}\right)\left(\frac{d^2W}{dx^2}\right) - \frac{(e_0a)^4}{4} I_0\left(\frac{d^3U}{dx^3}\right)\left(\frac{dU}{dx}\right) + \frac{(e_0a)^4}{4} I_1\left(\frac{dU}{dx}\right)\left(\frac{d^4W}{dx^4}\right) - (e_0a)^2 \\ I_0(W)\left(\frac{d^2W}{dx^2}\right) - (e_0a)^2 I_1\left(\frac{d^2W}{dx^2}\right)\left(\frac{dU}{dx}\right) + (e_0a)^2 I_2\left(\frac{d^2W}{dx^2}\right)^2 + \frac{(e_0a)^4}{4} I_0\left(\frac{d^2W}{dx^2}\right)^2 \\ + \frac{(e_0a)^4}{4} I_1\left(\frac{d^2W}{dx^2}\right)\left(\frac{d^3U}{dx^3}\right) - \frac{(e_0a)^4}{4} I_2\left(\frac{d^2W}{dx^2}\right)\left(\frac{d^4W}{dx^4}\right) \end{array}\right] dx \qquad (32)$$

Where;

$$A_{11} = \frac{bh}{1-\upsilon^2}\left[\frac{(E_U - E_L)}{k+1} + E_L - \left(\frac{\vartheta}{2}\right)(E_U + E_L)\right]$$

$$B_{11} = \frac{bh^2k}{1-\upsilon^2}\left[\frac{(E_U - E_L)}{2(k+1)(k+2)}\right]$$

$$D_{11} = \frac{bh^3}{1-\upsilon^2}\left[\frac{(E_U - E_L)(k^2+k+2)}{4(k+1)(k+2)(k+3)} + \frac{E_L}{12} - \left(\frac{\vartheta}{24}\right)(E_U + E_L)\right]$$

$$I_0 = bh\left[\frac{(\rho_U - \rho_L)}{k+1} + \rho_L - \left(\frac{\vartheta}{2}\right)(\rho_U + \rho_L)\right]$$

$$I_1 = bh^2k\left[\frac{(\rho_U - \rho_L)}{2(k+1)(k+2)}\right]$$

$$I_2 = bh^3\left[\frac{(\rho_U - \rho_L)(k^2+k+2)}{4(k+1)(k+2)(k+3)} + \frac{\rho_L}{12} - \left(\frac{\vartheta}{24}\right)(\rho_U + \rho_L)\right]$$

Eq. (32) is the Lagrangian energy function of FG porous nanobeam with bi-Helmholtz type of nonlocal elasticity. The Lagrangian energy function for the Helmholtz type of nonlocal elasticity can be obtained from Eq. (32) as

$$\int_0^L \left[\begin{array}{l} A_{11}\left(\frac{dU}{dx}\right)^2 - 2B_{11}\left(\frac{d^2W}{dx^2}\right)\left(\frac{dU}{dx}\right) + D_{11}\left(\frac{d^2W}{dx^2}\right)^2 - (e_0a)^2 k_w \\ (W)\left(\frac{d^2W}{dx^2}\right) + (e_0a)^2 k_g \left(\frac{d^2W}{dx^2}\right)^2 + k_w W^2 + k_g\left(\frac{dW}{dx}\right)^2 \end{array} \right] dx$$
$$= \omega^2 \int_0^L \left[\begin{array}{l} I_0\left(U^2+W^2\right) - 2I_1(U)\left(\frac{dW}{dx}\right) + I_2\left(\frac{dW}{dx}\right)^2 + (e_0a)^2 I_0\left(\frac{dU}{dx}\right)^2 - (e_0a)^2 I_1\left(\frac{dU}{dx}\right) \\ \left(\frac{d^2W}{dx^2}\right) - (e_0a)^2 I_0 (W)\left(\frac{d^2W}{dx^2}\right) - (e_0a)^2 I_1\left(\frac{d^2W}{dx^2}\right)\left(\frac{dU}{dx}\right) + (e_0a)^2 I_2\left(\frac{d^2W}{dx^2}\right)^2 \end{array} \right] dx \tag{33}$$

3.2 Equation of motion for Navier's technique

Substituting Eq. (25) into Eq. (23), the governing equations of motion in terms of displacement can be obtained as

$$\left\{ \begin{array}{l} A_{11}\left(\frac{\partial^2 u}{\partial x^2}\right) - B_{11}\left(\frac{\partial^3 w}{\partial x^3}\right) = I_0\left(\frac{\partial^2 u}{\partial t^2}\right) - I_1\left(\frac{\partial^3 w}{\partial x \partial t^2}\right) - (e_0a)^2 \\ \left\{ I_0\left(\frac{\partial^4 u}{\partial x^2 \partial t^2}\right) - I_1\left(\frac{\partial^5 w}{\partial x^3 \partial t^2}\right)\right\} + \frac{(e_0a)^4}{4}\left\{ I_0\left(\frac{\partial^6 u}{\partial x^4 \partial t^2}\right) - I_1\left(\frac{\partial^7 w}{\partial x^5 \partial t^2}\right)\right\} \end{array} \right\} \tag{34.a}$$

$$\left\{ \begin{array}{l} B_{11}\left(\frac{\partial^3 u}{\partial x^3}\right) - D_{11}\left(\frac{\partial^4 w}{\partial x^4}\right) = I_0\left(\frac{\partial^2 w}{\partial t^2}\right) + I_1\left(\frac{\partial^3 u}{\partial x \partial t^2}\right) - I_2\left(\frac{\partial^4 w}{\partial x^2 \partial t^2}\right) + k_w w - k_g\left(\frac{\partial^2 w}{\partial x^2}\right) - \\ (e_0a)^2 \left\{ \begin{array}{l} I_0\left(\frac{\partial^4 w}{\partial x^2 \partial t^2}\right) + I_1\left(\frac{\partial^5 u}{\partial x^3 \partial t^2}\right) - I_2 \\ \left(\frac{\partial^6 w}{\partial x^4 \partial t^2}\right) + k_w\left(\frac{\partial^2 w}{\partial x^2}\right) - k_g\left(\frac{\partial^4 w}{\partial x^4}\right) \end{array} \right\} + \frac{(e_0a)^4}{4} \left\{ \begin{array}{l} I_0\left(\frac{\partial^6 w}{\partial x^4 \partial t^2}\right) + I_1\left(\frac{\partial^7 u}{\partial x^5 \partial t^2}\right) - I_2 \\ \left(\frac{\partial^8 w}{\partial x^6 \partial t^2}\right) + k_w\left(\frac{\partial^4 w}{\partial x^4}\right) - k_g\left(\frac{\partial^6 w}{\partial x^6}\right) \end{array} \right\} \end{array} \right\} \tag{34.b}$$

The governing equations of motion for the Helmholtz type of nonlocal elasticity can be obtained from Eq. (34) as

$$A_{11}\left(\frac{\partial^2 u}{\partial x^2}\right) - B_{11}\left(\frac{\partial^3 w}{\partial x^3}\right) = I_0\left(\frac{\partial^2 u}{\partial t^2}\right) - I_1\left(\frac{\partial^3 w}{\partial x \partial t^2}\right) - (e_0a)^2\left\{ I_0\left(\frac{\partial^4 u}{\partial x^2 \partial t^2}\right) - I_1\left(\frac{\partial^5 w}{\partial x^3 \partial t^2}\right)\right\} \tag{35.a}$$

$$B_{11}\left(\frac{\partial^3 u}{\partial x^3}\right)-D_{11}\left(\frac{\partial^4 w}{\partial x^4}\right)=I_0\left(\frac{\partial^2 w}{\partial t^2}\right)+I_1\left(\frac{\partial^3 u}{\partial x\partial t^2}\right)-I_2\left(\frac{\partial^4 w}{\partial x^2\partial t^2}\right)+k_w w-k_g\left(\frac{\partial^2 w}{\partial x^2}\right)$$
$$-(e_0 a)^2\left\{I_0\left(\frac{\partial^4 w}{\partial x^2\partial t^2}\right)+I_1\left(\frac{\partial^5 u}{\partial x^3\partial t^2}\right)-I_2\left(\frac{\partial^6 w}{\partial x^4\partial t^2}\right)+k_w\left(\frac{\partial^2 w}{\partial x^2}\right)-k_g\left(\frac{\partial^4 w}{\partial x^4}\right)\right\} \tag{35.b}$$

4. Solution procedures

In the upcoming subsections, the Hermite-Ritz method and Navier's technique have been described to solve the governing equations of motion for the proposed model.

4.1 Application of Hermite-Ritz method

Hermite polynomials [Bay□n and Bayin 2006] $(H(n,x))$ are set of orthogonal polynomials with respect to the weight function e^{-x^2} defined over the domain $(-\infty,\infty)$, i.e.,

$$\int_{-\infty}^{\infty} e^{-x^2} H(m,x)H(n,x)dx=\begin{cases}\sqrt{\pi}\,2^n n!, & n=m\\ 0, & n\neq m\end{cases} \tag{36}$$

First five terms of Hermite polynomials with recurrence relations can be expressed as [Bay□n and Bayin 2006]

$H(0,x)=1$

$H(1,x)=2x$

$H(2,x)=4x^2-2$

$H(3,x)=8x^3-12x$

$H(4,x)=16x^4-48x^2+12$

$$H(n,x)=2xH(n-1,x)-2(n-1)H(n-2,x) \text{ and } H'(n,x)=2nH(n-1,x) \tag{37}$$

In this investigation, Hermite polynomials are taken as shape functions, i.e., both the axial and transverse displacements of the FG nanobeam are expressed in terms of Hermite polynomials. The main reasons behind choosing the Hermite polynomials as shape functions are;

- Hermite polynomials are the orthogonal polynomials which reduce the computation time.

- Unlike other orthogonal polynomials such as Chebyshev polynomials, Legendre polynomials, etc., the domain is $(-\infty, \infty)$ that offers flexibility in the limit of the Lagrangian energy function.
- It helps to restrict ill-conditioning of the matrix for higher values of polynomials.

The axial displacement $U(X)$, and transverse displacement $W(X)$ can be now expressed as [Pradhan and Chakraverty 2014]

$$U(X) = X^{\eta}(R-X)^{\kappa}\sum_{i=1}^{n} c_i H(i-1, X) \tag{38.a}$$

$$W(X) = X^{\eta}(R-X)^{\kappa}\sum_{i=1}^{n} d_i H(i-1, X) \tag{38.b}$$

Here c_i's, and d_i's are unknown coefficients, $H(n, X)$ is the nth term of Hermite polynomial which is used shape function, $X^{\eta}(R-X)^{\kappa}$ is the admissible functions with exponents η, and κ. For different boundary conditions η, and κ possess different values, as shown in Table 1.

Table 1 η, and κ for different boundary conditions [Pradhan and Chakraverty 2014].

B.C.	η	κ
H-H	1	1
C-H	2	1
C-C	2	2

Substituting Eq. (38) into the Lagrangian energy function of bi-Helmholtz and Helmholtz types of nonlocal elasticity, i.e., Eq.(32) and Eq.(33) and minimizing Ω^2 with respect to the unknown coefficients c_i's, and d_i's, $i = 1,2,3\ldots n$, give rise to the generalized eigenvalue problem as

$$[\mathrm{K}]\{X\} = \Omega^2 [\mathrm{M}]\{X\} \tag{39}$$

where $\{X\} = [c_1, c_2, c_3, \ldots c_n, d_1, d_2, d_3, \ldots d_n]^T$, $[\mathrm{K}]$ represents the stiffness matrix, and $[\mathrm{M}]$ denotes the mass matrix.

4.2 Application of Navier's technique

As per the Navier's technique the axial displacement $u(x,t)$ and transverse the displacement $w(x,t)$ can be expanded in terms of sine and cosine series as [Bekhadda et al. 2019];

$$u\ (x,t)=\sum_{m=1}^{\infty}u_m\cos\left(\frac{m\pi}{L}x\right)e^{i\omega t} \tag{40.a}$$

$$w(x,t)=\sum_{m=1}^{\infty}w_m\sin\left(\frac{m\pi}{L}x\right)e^{i\omega t} \tag{40.b}$$

where u_m and w_m are arbitrary parameters and ω is the natural frequency of vibration. Plugging Eq. (40) into the Eq. (34), and Eq. (35), generalized Eigenvalue problem for free vibration of FG nanobeam for bi- Helmholtz and Helmholtz types nonlocal elasticity, respectively, will be obtained as

$$\left[\mathrm{K}^{bH}\right]\{X\}=\omega^2\left[\mathrm{M}^{bH}\right]\{X\} \tag{41.a}$$

$$\left[\mathrm{K}^{H}\right]\{X\}=\omega^2\left[\mathrm{M}^{H}\right]\{X\} \tag{41.b}$$

Here $\left[K^{bH}\right]=\begin{bmatrix}k_{11} & k_{12}\\ k_{21} & k_{22}\end{bmatrix}$, $\left[\mathrm{M}^{bH}\right]=\begin{bmatrix}m_{11} & m_{12}\\ m_{21} & m_{22}\end{bmatrix}$, $\left[K^{H}\right]=\begin{bmatrix}\bar{k}_{11} & \bar{k}_{12}\\ \bar{k}_{21} & \bar{k}_{22}\end{bmatrix}$, $\left[\mathrm{M}^{H}\right]=\begin{bmatrix}\bar{m}_{11} & \bar{m}_{12}\\ \bar{m}_{21} & \bar{m}_{22}\end{bmatrix}$ and $\{X\}=\begin{bmatrix}u_m & w_m\end{bmatrix}^T$,

where;

$$k_{11}=-A_{11}\left(\frac{m\pi}{L}\right)^2,\ k_{12}=k_{21}=B_{11}\left(\frac{m\pi}{L}\right)^3,$$

$$k_{22}=-D_{11}\left(\frac{m\pi}{L}\right)^4-(k_w)-(k_g)\left(\frac{m\pi}{L}\right)^2-(e_0a)^2(k_w)\left(\frac{m\pi}{L}\right)^2$$
$$-(e_0a)^2(k_g)\left(\frac{m\pi}{L}\right)^4-\frac{(e_0a)^4}{4}(k_w)\left(\frac{m\pi}{L}\right)^4-\frac{(e_0a)^4}{4}(k_g)\left(\frac{m\pi}{L}\right)^6,$$

$$m_{11}=-I_0-(e_0a)^2(I_0)\left(\frac{m\pi}{L}\right)^2-\frac{(e_0a)^4}{4}(I_0)\left(\frac{m\pi}{L}\right)^4,$$

$$m_{12}=m_{21}=I_1\left(\frac{m\pi}{L}\right)+(e_0a)^2(I_1)\left(\frac{m\pi}{L}\right)^3+\frac{(e_0a)^4}{4}(I_1)\left(\frac{m\pi}{L}\right)^5,$$

$$m_{22} = -I_0 - I_2\left(\frac{m\pi}{L}\right)^2 - I_0(e_0a)^2\left(\frac{m\pi}{L}\right)^2 - I_2(e_0a)^2$$
$$\left(\frac{m\pi}{L}\right)^4 - I_0\frac{(e_0a)^4}{4}\left(\frac{m\pi}{L}\right)^4 - I_2\frac{(e_0a)^4}{4}\left(\frac{m\pi}{L}\right)^6 ,$$

$$\bar{k}_{11} = -A_{11}\left(\frac{m\pi}{L}\right)^2,\ \bar{k}_{12} = \bar{k}_{21} = B_{11}\left(\frac{m\pi}{L}\right)^3,$$

$$\bar{k}_{22} = -D_{11}\left(\frac{m\pi}{L}\right)^4 - (k_w) - (k_g)\left(\frac{m\pi}{L}\right)^2 - (e_0a)^2(k_w)\left(\frac{m\pi}{L}\right)^2 - (e_0a)^2(k_g)\left(\frac{m\pi}{L}\right)^4,$$

$$\bar{m}_{11} = -I_0 - (e_0a)^2(I_0)\left(\frac{m\pi}{L}\right)^2,\ \bar{m}_{12} = \bar{m}_{21} = I_1\left(\frac{m\pi}{L}\right) + (e_0a)^2(I_1)\left(\frac{m\pi}{L}\right)^3,$$

$$\bar{m}_{22} = -I_0 - I_2\left(\frac{m\pi}{L}\right)^2 - I_0(e_0a)^2\left(\frac{m\pi}{L}\right)^2 - I_2(e_0a)^2\left(\frac{m\pi}{L}\right)^4.$$

By solving the Eigenvalue problem mentioned in Eq. (41), the natural frequencies for the proposed model will be obtained for Hinged-Hinged (HH) boundary condition.

5. Numerical results and discussions

In this investigation, the FG nanobeam is considered to be composed of metal constituents as alpha-beta titanium alloy or titanium (Ti-6AL-4V) and ceramic constituent as zirconia or zirconium dioxide (ZrO_2). The geometrical properties or dimension of the specimen is taken from [Uzun and Yayl□ 2020] as width $(b) = 400nm$, thickness $(h) = 100nm$, and length $(L) = 8000nm$, whereas the mechanical properties [Uzun and Yayl□ 2020] are given as;

zirconia or zirconium dioxide (ZrO_2): $E_U = 151GPa$, $\rho_U = 3000\,Kg.m^{-3}$, and $\upsilon_U = 0.3$

titanium (Ti-6AL-4V): $E_L = 105.7\,GPa$, $\rho_L = 4429\,Kg.m^{-3}$, and $\upsilon_L = 0.298$.

The Young's modulus and mass density are assumed to vary through the thickness in accordance with the power-law exponent model. At the same time, for the sake of convenience, the Poisson's ratio is taken constant throughout the thickness of the FG nanobeam, which is $\upsilon = 0.3$.

5.1 Validation

In this subsection, the validation of the present model has been conducted with other existing results in special cases. In this regard, the first three natural frequencies of the functionally graded nanobeam of HH boundary condition has been compared with [Uzun and Yayl□ 2020], by neglecting the porosity and assuming Helmholtz nonlocal operator. The numerical results are computed for HH boundary condition by using both the Navier's technique (NT) and the Hermite-Ritz method (H-RM), which is demonstrated in Table 2. Likewise, the fundamental frequency parameter $\left(\lambda = \frac{\omega L^2}{h}\sqrt{\frac{\rho_L}{E_L}}\right)$ for HH boundary condition has been compared with [Pradhan and Chakraverty 2014; Aydogdu and Taskin 2007] by neglecting the porosity, nonlocal effect, and elastic foundation. Here the material is considered as Alumina (Al_2O_3), and Aluminum (Al), and the gradation is taken along Young's modulus only with $E_L = 70\,\text{GPa}$, $E_U = 380\,\text{GPa}$ and $\upsilon = 0.3$. The tabular result is depicted in Table 3, with various power-law exponent and aspect ratio. From these results, it is evident that the present model is accurate and copes well with the existing results in special cases.

Table 2 Comparison of natural frequencies (in MHz) obtained by present study with Uzun and Yayl□ [2020], in special cases

(α)	k	ω_1			ω_2			ω_3		
		[A]	Present (NT)	Present (H-RM)	[A]	Present (NT)	Present (H-RM)	[A]	Present (NT)	Present (H-RM)
0	0	10.2084	10.3295	10.3294	26.4247	27.1637	27.1640	51.9523	53.8340	54.5844
	2	8.6973	8.7744	8.7835	21.7885	22.2755	22.2756	42.0585	43.3202	43.9188
	4	8.4672	8.5437	8.5497	21.1040	21.5893	21.5894	40.6136	41.8749	42.4450
	6	8.3682	8.4449	8.4488	20.7909	21.2794	21.2795	39.9342	41.2065	41.7618
	8	8.3116	8.3883	8.3910	20.6024	21.0920	21.0921	39.5165	40.7935	41.3395
0.2	0	9.8519	9.9418	9.9418	21.2306	21.5871	21.5873	33.1951	33.8385	34.2605
	2	8.4376	8.4945	8.5012	17.9078	18.1366	18.1367	27.8374	28.2510	28.6052
	4	8.2208	8.2772	8.2816	17.4076	17.6348	17.6350	27.0354	27.4468	27.7885
	6	8.1285	8.1851	8.1880	17.1877	17.4160	17.4162	26.6971	27.0928	27.4283
	8	8.0763	8.1329	8.1349	17.0597	17.2882	172884	26.4697	26.8839	27.2159
0.4	0	9.4203	9.4710	9.4709	18.6882	18.8290	18.8292	28.0525	28.2723	28.6346
	2	8.1250	8.1568	8.1605	16.0475	16.1355	16.1357	24.0603	24.1955	24.5070
	4	7.9245	7.9559	7.9584	15.6414	15.7285	15.7287	23.4472	23.5814	23.8843

	6	7.8405	7.8721	7.8737	15.4695	15.5570	15.5572	23.1871	23.3220	23.6210
	8	7.7938	7.8253	7.8264	15.3729	15.4603	15.4605	23.0405	23.1754	23.4721

A: Uzun and Yayl□ [2020]

Table 3 Comparison of frequency parameters obtained by present study with Pradhan and Chakraverty [2014], Aydogdu and Taskin [2007], in special cases

$\left(L/h\right)$	k	0	0.1	1	2	10
5	[C]	6.847	6.499	4.821	4.251	3.737
	[B]	6.847	6.512	5.176	4.752	3.959
	Present	6.8470	6.5120	5.1764	4.7518	3.9597
20	[C]	6.951	6.599	4.907	4.334	3.804
	[B]	6.951	6.612	5.256	4.826	4.021
	Present	6.9516	6.6115	5.2562	4.8258	4.0208

B: Pradhan and Chakraverty [2014]

C: Aydogdu and Taskin [2007]

5.2 Convergence

Through this subsection, the convergence of the present model has been carried out for first four natural frequencies of FG nanobeam by considering the power-law exponent $(k)=1$, porosity volume fraction $(\vartheta)=0.1$, non-dimensional nonlocal parameter $\alpha=\left(e_0a/L\right)=0.1$, non-dimensional Winkler elastic constant $K_w=\left(k_wL^4/E_LI\right)=40$, and non-dimensional Pasternak elastic constant $K_g=\left(k_gL^2/E_LI\right)=40$. Variations of the first four natural frequencies have studied with no. of terms of the Hermite polynomial for HH, CH, and CC boundary conditions, which are depicted in Fig. (4), Fig. (5), and Fig. (6), respectively. Natural frequencies have also been computed from the closed-form solution by using Navier's technique (NT) for HH boundary condition and compared with the results of the Hermite-Ritz method (HRM) showing good agreement as illustrated in Fig. 4. From these graphical results, it is quite evident that the first four natural frequencies of all the boundary conditions are attaining the convergence on or after no. of terms $(n)=6$. Also, it may be observed that the CC boundary condition is approaching convergence faster than HH and CH boundary conditions.

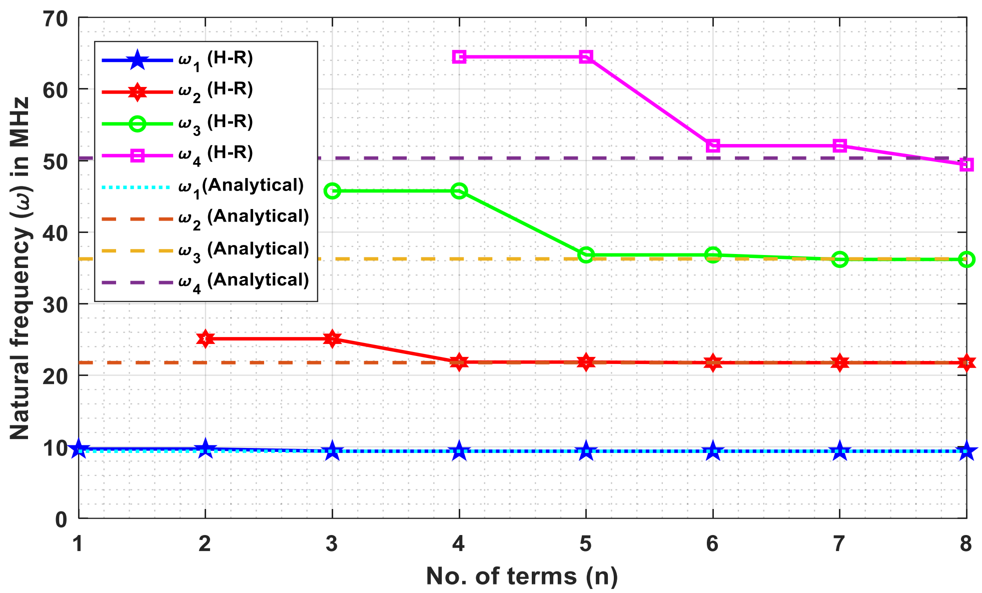

Fig. 4 Variation of first four natural frequencies (ω) with no. of terms (n) and comparison with analytical results for HH boundary condition

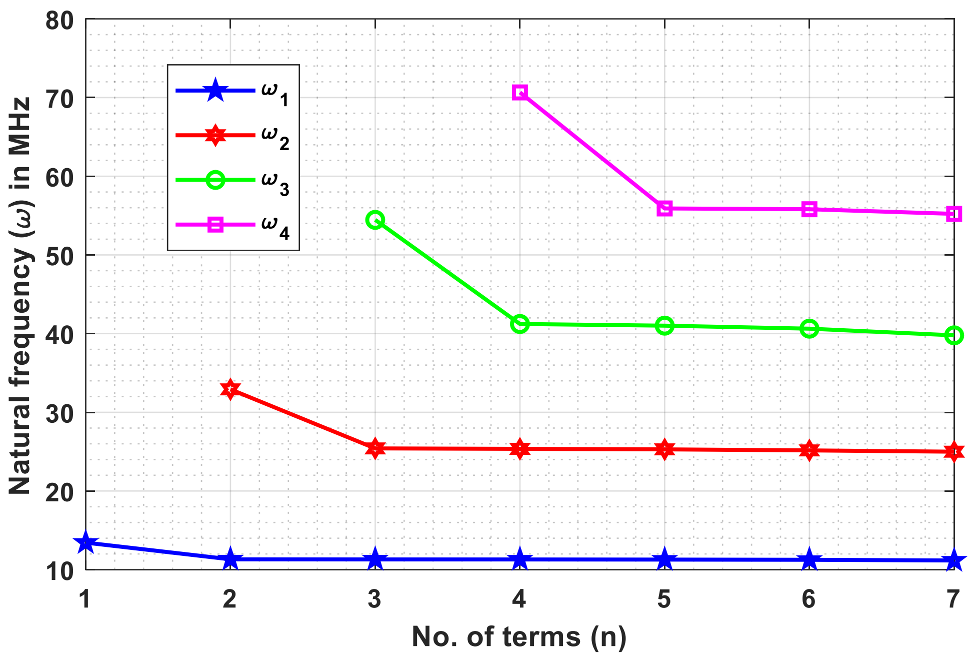

Fig. 5 Variation of first four natural frequencies (ω) with no. of terms (n) for CH boundary condition

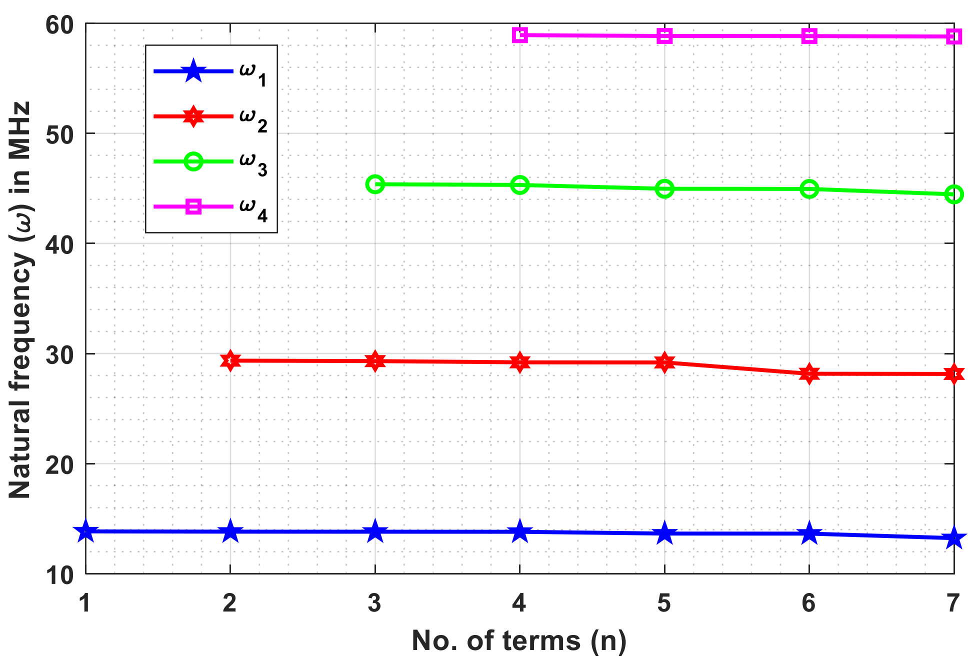

Fig. 6 Variation of first four natural frequencies (ω) with no. of terms (n) for CC boundary condition

5.3 Effect of bi-Helmholtz nonlocal elasticity

In this subsection, the influence of the bi-Helmholtz operator has been studied on natural frequencies of HH, CH, and CC boundary conditions as compared with the Helmholtz operator. For the computational purpose, power-law exponent $(k)=1$, porosity volume fraction $(\vartheta)=0.1$, non-dimensional Winkler elastic constant $(K_w)=40$, and non-dimensional Winkler elastic constant $(K_g)=40$ are taken into consideration. The graphical results, i.e., Fig. 7.a, and Fig. 7.b represents the variation of first four natural frequencies with respect to the nonlocal parameters (α) for bi-Helmholtz and Helmholtz operators, respectively, for HH boundary condition, and these results are computed by employing Navier's technique. Likewise, Fig. 8 and Fig. 9 illustrate the graphical results for CH and CC boundary conditions, respectively, which are computed using the Hermite-Ritz method. Here, the nonlocal parameters are assumed to vary from 0 to 0.5 with an increment of 0.1. From these graphical results, it may clear that the natural frequencies for all modes and all boundary conditions are decreasing with increase in nonlocal parameters except for the first and second modes of CH and CC boundary conditions with respect to bi-Helmholtz operator. Also, this decrease is very significant in the case of higher modes.

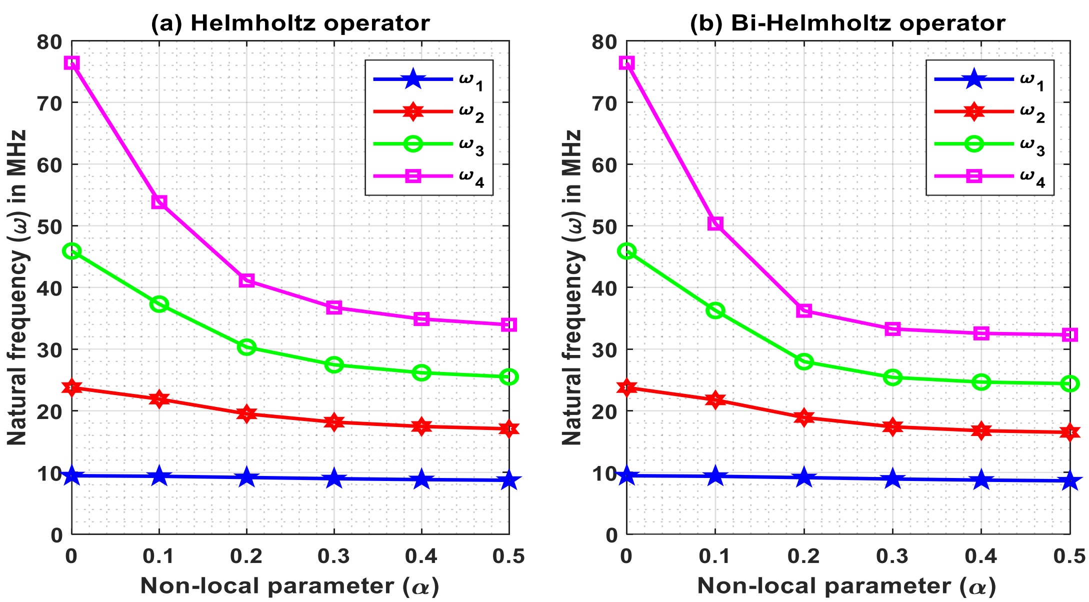

Fig. 7 Variation of first four natural frequencies (ω) with nonlocal parameter (α) for HH boundary condition

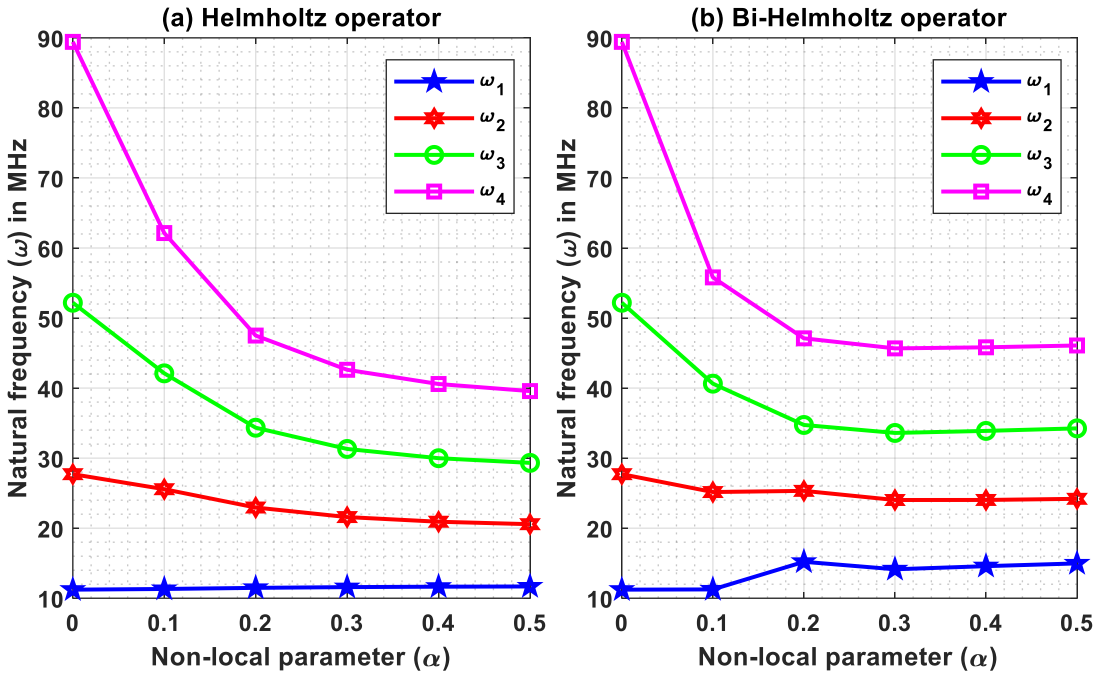

Fig. 8 Variation of first four natural frequencies (ω) with nonlocal parameter (α) for CH boundary condition

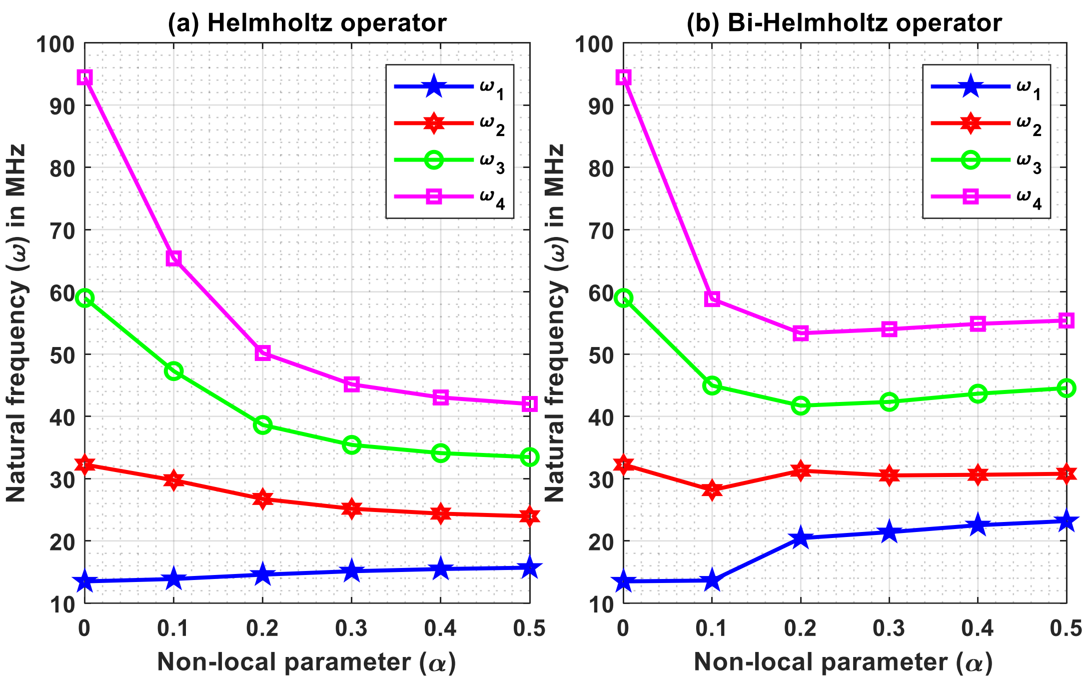

Fig. 9 Variation of first four natural frequencies (ω) with nonlocal parameter (α) for CC boundary condition

5.4 Effect of porosity or porosity volume fraction index

This subsection is dedicated to investigating the effect of porosity or porosity vol. fraction index (ϑ) on natural frequencies of FG porous nanobeam. Here the porosity vol. fraction (ϑ) is varied from 0 to 0.5 with an increase of 0.1, and other scaling parameters are taken as; power-law exponent $(k)=1$, non-dimensional nonlocal parameter $(\alpha)=0.1$ non-dimensional Winkler elastic foundation $(K_w)=40$, and non-dimensional Pasternak elastic foundation $(K_g)=40$. In this regard, graphical and tabular results are given in Table 4 and Figs. 10-12. Natural frequencies of the FG nanobeam increase with the rise in porosity index, which is applicable for all modes, all boundary conditions, and in the case of both the bi-Helmholtz and Helmholtz operators. This is because although with more value of porosity parameter the stiffness of beam becomes lesser and also its cross-sectional moment of inertia reduces, the reduction rate of inertia is more than that of the stiffness in the beam. It should be noted that other types of porosity may have opposite result. Also, it may be noted that the increase in natural frequencies is more significant in higher modes. The results obtained by both the bi-Helmholtz and Helmholtz operators are almost equal in lower modes where it can be clearly distinguished for higher modes, Helmholtz operator possesses more natural frequencies than bi-Helmholtz, and this trend is valid in all the boundary conditions.

Table 4 Natural frequencies (MHz) for Helmholtz operator (Ho) and Bi-Helmholtz operators (B-Ho) with respect to porosity volume fraction index.

(a) Hinged-Hinged (HH) boundary condition

Porosity ϑ	ω_1		ω_2		ω_3		ω_4	
	Ho	**B-Ho**	**Ho**	**B-Ho**	**Ho**	**B-Ho**	**Ho**	**B-Ho**
0	8.9954	8.9933	21.2976	21.1592	36.5307	35.4690	52.9015	49.3444
0.1	9.3787	9.3766	21.8957	21.7614	37.2957	36.2590	53.8264	50.3436
0.2	9.8364	9.8345	22.6194	22.4899	38.2265	37.2193	54.9544	51.5600
0.3	10.3948	10.3930	23.5144	23.3904	39.3847	38.4129	56.3614	53.0744
0.4	11.0950	11.0933	24.6526	24.5353	40.8676	39.9393	58.1674	55.0143
0.5	12.0053	12.0038	26.1546	26.0456	42.8384	41.9655	60.5741	57.5937

(b) Clamped-Hinged (CH) boundary condition

Porosity ϑ	ω_1		ω_2		ω_3		ω_4	
	Ho	**B-Ho**	**Ho**	**B-Ho**	**Ho**	**B-Ho**	**Ho**	**B-Ho**
0	10.9378	10.8823	24.9546	24.5642	41.3135	39.8005	61.1409	54.8442
0.1	11.3221	11.2586	25.5648	25.1599	42.1072	40.6310	62.1339	55.8055
0.2	11.7839	11.7097	26.3055	25.8800	43.0744	41.6392	63.3464	56.9640
0.3	12.3509	12.2622	27.2248	26.7690	44.2801	42.8905	64.8610	58.3899
0.4	13.0667	12.9572	28.3985	27.8965	45.8267	44.4877	66.8086	60.1930
0.5	14.0039	13.8634	29.9541	29.3777	47.8868	46.6030	69.4088	62.5552

(c) Clamped-Clamped (CC) boundary condition

Porosity ϑ	ω_1		ω_2		ω_3		ω_4	
	Ho	**B-Ho**	**Ho**	**B-Ho**	**Ho**	**B-Ho**	**Ho**	**B-Ho**
0	13.4994	13.2904	29.1138	27.7048	46.4458	44.1091	64.3550	57.9714
0.1	13.8795	13.6388	29.7438	28.1601	47.2742	44.9480	65.3712	58.8354
0.2	14.3390	14.0564	30.5101	28.6844	48.2846	45.9578	66.6120	59.7990
0.3	14.9070	14.5671	31.4636	29.2890	49.5452	47.1975	68.1620	60.8655
0.4	15.6290	15.2076	32.6841	29.9802	51.1640	48.7578	70.1544	62.0347
0.5	16.5814	16.0379	34.3065	30.7424	53.3224	50.7858	72.8136	63.3195

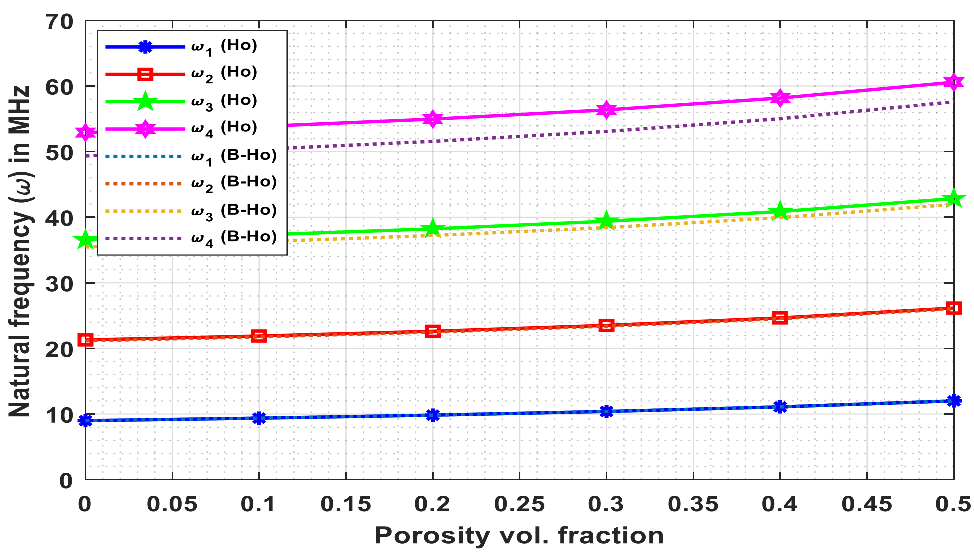

Fig. 10 Variation of first four natural frequencies (ω) with porosity vol. fraction index (ϑ) for HH boundary condition

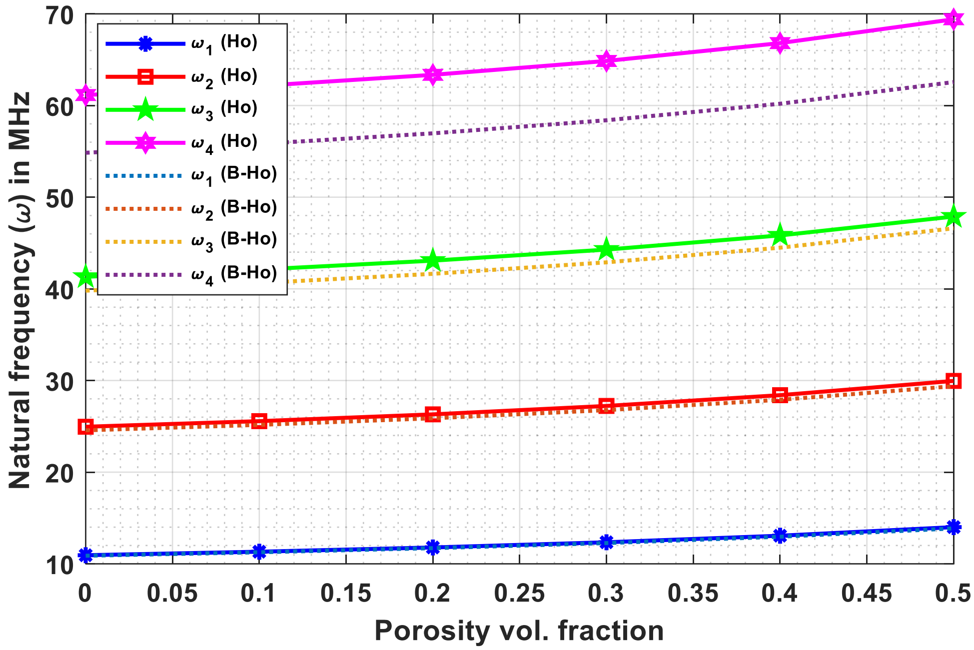

Fig. 11 Variation of first four natural frequencies (ω) with porosity vol. fraction index (ϑ) for CH boundary condition

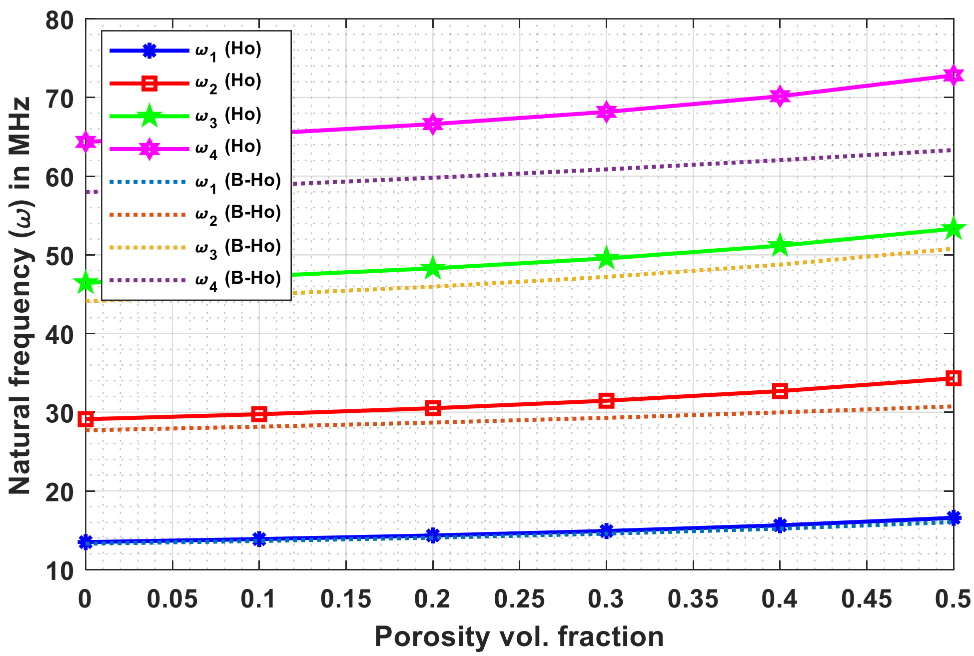

Fig. 12 Variation of first four natural frequencies (ω) with porosity vol. fraction index (ϑ) for CC boundary condition

5.5 Effect of Power-law exponent

In this subsection, the influence of the power-law exponent (k) has been studied on the natural frequencies of FG nanobeam. The power-law exponent (k) is taken as 0, 0.2, 0.5, 1, 2, 3, 5, with porosity volume fraction $(\vartheta)=0.1$, non-dimensional parameter $(\alpha)=0.1$, non-dimensional Winkler elastic constant $(K_w)=40$, and non-dimensional Pasternak elastic constant $(K_g)=40$. Table 5(a-c) and Figs. (13-15) represent the tabular and graphical results for HH, CH, and CC edges with respect to both the bi-Helmholtz and Helmholtz operators. All the computations for HH edge are carried out by using Navier's technique, while the Hermite-Ritz method is used for other boundary conditions. These results clearly reveals that the natural frequencies of all modes and all boundary conditions decrease with an increase in the power-law exponent (k), that means when the beam is purely ceramic i.e., at $k=0$ possesses the highest natural frequencies and when the beam is purely metal i.e., at $k=\infty$ retains the lowest natural frequencies. This reduction is due to the fact that as we go on increasing the power-law exponent (k), the beam becomes more flexible, retaining less natural frequencies. This reduction is more remarkable with higher modes and at $k<2$.

Table 5 Natural frequencies (MHz) for Helmholtz operator and Bi-Helmholtz operator with respect to power-law index.

(a) Hinged-Hinged (HH) boundary condition

k	ω_1		ω_2		ω_3		ω_4	
	Ho	**B-Ho**	**Ho**	**B-Ho**	**Ho**	**B-Ho**	**Ho**	**B-Ho**
0	10.7925	10.7898	25.8422	25.6668	44.5660	43.2276	64.7052	60.2300
0.2	10.2533	10.2509	24.3164	24.1573	41.7427	40.5234	60.4730	56.3892
0.5	9.7849	9.7827	23.0058	22.8605	39.3257	38.2072	56.8548	53.1023
1	9.3787	9.3766	21.8957	21.7614	37.2957	36.2590	53.8264	50.3436
2	9.0255	9.0236	20.9608	20.8352	35.6073	34.6351	51.3214	48.0518
3	8.8637	8.8619	20.5373	20.4155	34.8459	33.9022	50.1941	47.0188
5	8.7060	8.7042	20.1140	19.9962	34.0766	33.1631	49.0495	45.9742

(b) Clamped-Hinged (CH) boundary condition

k	ω_1		ω_2		ω_3		ω_4	
	Ho	**B-Ho**	**Ho**	**B-Ho**	**Ho**	**B-Ho**	**Ho**	**B-Ho**
0	13.1944	13.1310	30.3566	29.8811	50.4572	48.5432	74.8310	67.0271
0.2	12.4736	12.4098	28.4981	28.0498	47.2095	45.4679	69.8833	62.6547
0.5	11.8530	11.7892	26.9066	26.4819	44.4338	42.8388	65.6618	58.9263
1	11.3221	11.2586	25.5648	25.1599	42.1072	40.6310	62.1339	55.8055
2	10.8668	10.8035	24.4403	24.0509	40.1747	38.7905	59.2147	53.2083
3	10.6584	10.5948	23.9305	23.5472	39.3021	37.9573	57.8970	52.0277
5	10.4516	10.3871	23.4172	23.0390	38.4169	37.1130	56.5535	50.8202

(c) Clamped-Clamped (CC) boundary condition

k	ω_1		ω_2		ω_3		ω_4	
	Ho	**B-Ho**	**Ho**	**B-Ho**	**Ho**	**B-Ho**	**Ho**	**B-Ho**
0	16.3750	16.1390	35.4890	33.8613	56.7848	53.8613	78.8026	70.9212
0.2	15.4095	15.1707	33.2565	31.6420	53.0834	50.3948	73.5705	66.2187
0.5	14.5811	14.3408	31.3478	29.7477	49.9212	47.4324	69.1034	62.2012
1	13.8795	13.6388	29.7438	28.1601	47.2742	44.9480	65.3712	58.8354
2	13.2872	13.0467	28.4052	26.8338	45.0807	42.8800	62.2886	56.0261
3	13.0181	12.7767	27.7990	26.2265	44.0912	41.9427	60.9000	54.7382
5	12.7484	12.5044	27.1856	25.5997	43.0856	40.9884	59.4853	53.4032

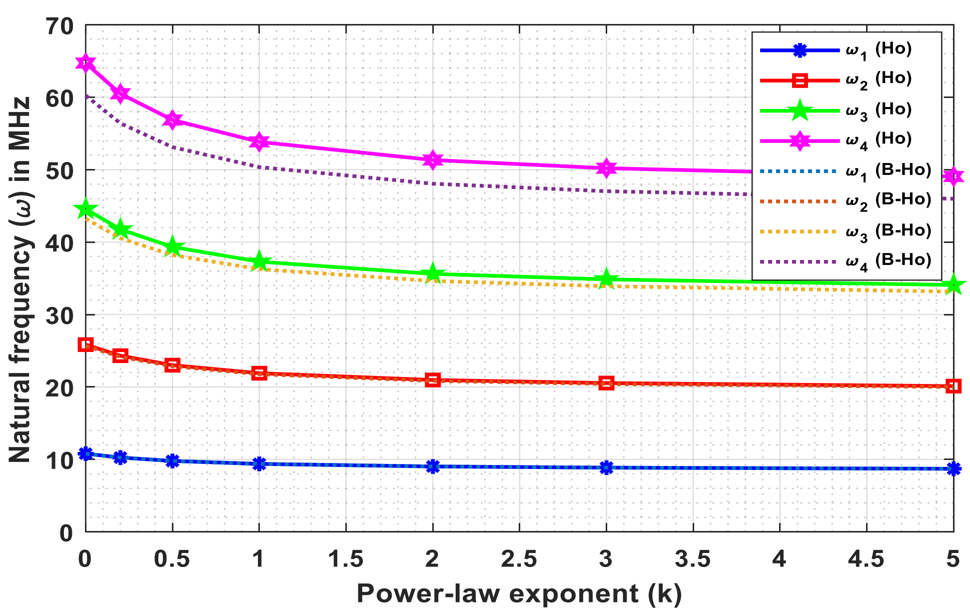

Fig. 13 Variation of first four natural frequencies (ω) with power-law index (k) for HH edge

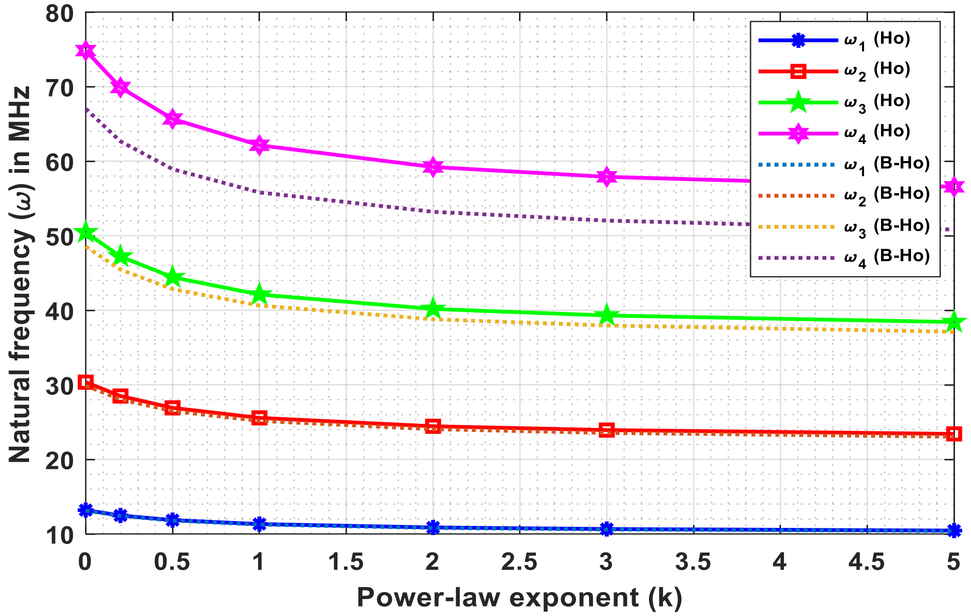

Fig. 14 Variation of first four natural frequencies (ω) with power-law index (k) for CH edge

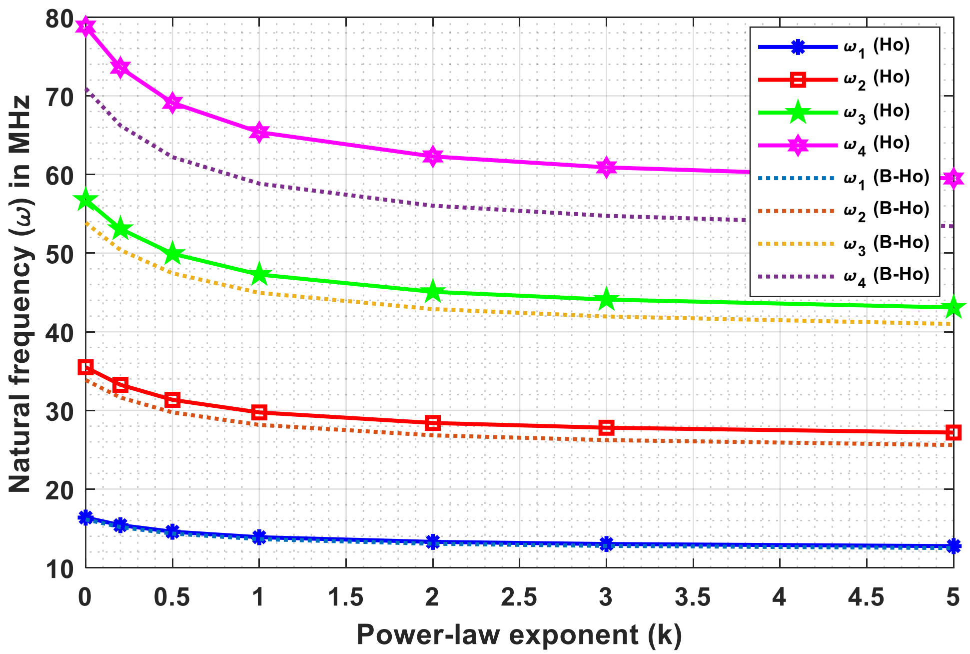

Fig. 15 Variation of first four natural frequencies (ω) with power-law index (k) for CC edge

5.6 Effect of elastic foundation

This subsection is devoted to analyzing the effect of elastic foundation, i.e., non-dimensional Winkler(K_w), and Pasternak(K_g) elastic parameters on natural frequencies of the FG nanobeam. In this regard, a comprehensive study has been undertaken by varying the elastic parameters, and the results are noted in tabular form, which can be seen in Table 6. The tabular results are incorporated for HH, CH, and CC boundary conditions with power-law exponent $(k)=1$, porosity volume fraction$(\vartheta)=0.1$, and nonlocal parameter$(\alpha)=0.1$. Different combinations for elastic foundations are considered, and results are noted for the first four natural frequencies by considering both bi-Helmholtz and Helmholtz operators. From these results, it's quite clear that the natural frequencies increase with the increase in elastic constants except the second mode of CC edge, where some irregularities occur with few combinations for elastic foundations, and these growths are more remarkable with higher modes. The increase in natural frequencies can be explained by the fact that the higher values of elastic parameters make the beam stiffer resulting higher value of natural frequencies.

Table 6 Natural frequencies (MHz) for Helmholtz operator and Bi-Helmholtz operator with respect to elastic foundation

(a) Hinged-Hinged (HH) boundary condition

(K_w, K_g)	ω_1		ω_2		ω_3		ω_4	
	Ho	B-Ho	Ho	B-Ho	Ho	B-Ho	Ho	B-Ho
(0, 0)	4.1382	4.1336	14.6881	14.4871	28.3939	27.0178	43.1712	38.7421
(50, 0)	5.0270	5.0232	14.9627	14.7655	28.5369	27.1680	43.2652	38.8469
(100, 0)	5.7807	5.7774	15.2324	15.0387	28.6791	27.3173	43.3591	38.9514
(200, 0)	7.0504	7.0477	15.7579	15.5708	28.9614	27.6136	43.5462	39.1595
(500, 0)	9.9290	9.9270	17.2385	17.0676	29.7924	28.4839	44.1027	39.7774
(700, 0)	11.4529	11.4512	18.1587	17.9965	30.3338	29.0497	44.4698	40.1841
(1000, 0)	13.4180	13.4166	19.4575	19.3063	31.1281	29.8782	45.0149	40.7865
(0, 50)	9.8753	9.8734	23.1776	23.0508	39.1027	38.1152	56.1029	52.7706
(0, 100)	13.3386	13.3372	29.3030	29.2027	47.4534	46.6430	66.5682	63.7849
(0, 200)	18.4042	18.4032	38.7503	38.6746	60.8065	60.1762	83.6594	81.4622
(0, 500)	28.6548	28.6542	58.5692	58.5191	89.6340	89.2076	121.2501	119.7446

(0, 700)	33.8037	33.8031	68.6746	68.6319	104.5250	104.1596	140.8428	139.5489
(0, 1000)	40.3122	40.3118	81.5166	81.4807	123.5406	123.2316	165.9499	164.8531
(50, 50)	10.2795	10.2776	23.3526	23.2267	39.2066	38.2218	56.1753	52.8475
(100, 100)	13.9360	13.9346	29.5795	29.4803	47.6246	46.8171	66.6902	63.9123
(200, 200)	19.2691	19.2681	39.1683	39.0934	61.0736	60.4461	83.8535	81.6615
(500, 500)	30.0426	30.0420	59.2603	59.2108	90.0868	89.6626	121.5849	120.0836
(700, 700)	35.4504	35.4499	69.4996	69.4574	105.0685	104.7050	141.2463	139.9561
(10^3, 10^3)	42.2847	42.2842	82.5095	82.4740	124.1976	123.8902	166.4391	165.3455

(b) Clamped-Hinged (CH) boundary condition

(K_w, K_g)	ω_1		ω_2		ω_3		ω_4	
	Ho	B-Ho	Ho	B-Ho	Ho	B-Ho	Ho	B-Ho
(0, 0)	6.4253	6.4083	18.3745	17.9859	32.9521	30.8534	50.7756	43.9596
(50, 0)	7.0307	7.0151	18.5947	18.2108	33.0753	30.9850	50.8555	44.0520
(100, 0)	7.5879	7.5734	18.8124	18.4330	33.1981	31.1160	50.9354	44.1441
(200, 0)	8.5946	8.5819	19.2403	18.8696	33.4423	31.3764	51.0946	44.3278
(500, 0)	11.0789	11.0690	20.4705	20.1224	34.1643	32.1448	51.5695	44.8743
(700, 0)	12.4629	12.4541	21.2511	20.9160	34.6373	32.6470	51.8837	45.2350
(1000, 0)	14.2898	14.2821	22.3709	22.0528	35.3349	33.3862	52.3514	45.7707
(0, 50)	11.8992	11.8106	26.9144	26.4604	44.0082	42.5950	64.5997	58.1044
(0, 100)	15.5169	15.2826	33.3305	32.5184	52.8007	51.4876	75.9482	68.0455
(0, 200)	20.9356	20.3471	43.4007	41.5228	67.0109	65.4434	94.6476	80.4808
(0, 500)	32.0856	30.2815	64.8135	58.3572	97.9710	93.0027	136.1183	96.3964
(0, 700)	37.7273	35.0532	75.7982	65.7464	114.0332	101.8837	157.8232	111.2155
(0, 1000)	44.8781	40.8570	89.7895	74.2754	134.5788	114.0412	185.6826	130.8656
(50, 50)	12.2367	12.1506	27.0652	26.6138	44.1006	42.6904	64.6625	58.1743
(100, 100)	16.0332	15.8066	33.5739	32.7678	52.9545	51.6454	76.0551	68.1649
(200, 200)	21.6999	21.1326	43.7743	41.9131	67.2533	65.6915	94.8191	80.6828
(500, 500)	33.3308	31.5980	65.4386	59.0508	98.3853	93.4393	136.4165	96.8176
(700, 700)	39.2096	36.6439	76.5464	66.6078	114.5315	102.4415	158.1832	111.7264
(10^3, 10^3)	46.6579	42.8044	90.6917	75.3639	135.1820	114.7528	186.1197	131.4858

(c) Clamped-Clamped (CC) boundary condition

(K_w, K_g)	ω_1	ω_2	ω_3	ω_4

	Ho	B-Ho	Ho	B-Ho	Ho	B-Ho	Ho	B-Ho
(0, 0)	9.2819	9.2306	22.4127	21.7182	37.7523	34.6837	53.7256	45.8169
(50, 0)	9.7108	9.6618	22.5936	21.9048	37.8598	34.8008	53.8012	45.9054
(100, 0)	10.1215	10.0745	22.7731	22.0898	37.9671	34.9174	53.8766	45.9938
(200, 0)	10.8966	10.8529	23.1278	22.4553	38.1807	35.1496	54.0272	46.1700
(500, 0)	12.9463	12.9096	24.1607	23.5178	38.8145	35.8369	54.4764	46.6946
(700, 0)	14.1488	14.1152	24.8254	24.2002	39.2314	36.2880	54.7738	47.0411
(1000, 0)	15.7816	15.7515	25.7904	25.1892	39.8485	36.9542	55.2170	47.5562
(0, 50)	14.5242	14.1896	31.1770	29.0606	49.2867	46.9236	67.9123	60.6592
(0, 100)	18.2933	17.4110	37.9571	31.6656	58.5964	55.4373	79.6126	65.9577
(0, 200)	24.1051	21.9815	48.7571	27.9550	73.7730	67.9235	98.9483	74.2611
(0, 500)	36.3111	30.8467	72.0062	93.8346	107.0957	100.0219	141.9482	134.5057
(0, 700)	42.5415	35.2581	84.0015	107.3578	124.4489	114.8826	164.4844	155.6561
(0, 1000)	50.4634	40.8676	99.3133	124.8369	146.6785	134.3457	193.4267	182.9408
(50, 50)	14.8019	14.4738	31.3073	29.2003	49.3692	47.0102	67.9720	60.7262
(100, 100)	18.7332	17.8728	38.1710	31.9218	58.7350	55.5839	79.7146	66.0810
(200, 200)	24.7717	22.7106	49.0899	28.5321	73.9932	68.1627	99.1123	74.4800
(500, 500)	37.4159	32.1400	72.5693	94.2673	107.4748	100.4278	142.2341	134.8075
(700, 700)	43.8613	36.8399	84.6772	107.8871	124.9056	115.3773	164.8298	156.0211
(10^3, 10^3)	52.0525	42.8145	100.1296	125.4871	147.2320	134.9499	193.8462	183.3844

6. Concluding remarks

In this investigation, a computationally efficient method, namely the Hermite-Ritz method has been employed to compute the frequency response of the proposed model. Bi-Helmholtz type of nonlocal operator has been incorporated to seizure the effect small scale effect. HH, CH, and CC boundary conditions are considered in this investigation, and closed-form solution is also obtained for HH boundary condition by utilizing Navier's technique. Validation and convergence of the proposed model/and method have been conducted successfully. Conclusions obtained from the parametric study are summarized as follow;

- The natural frequencies are decreasing with the increase in the nonlocal parameters except for the first and second modes of CH and CC boundary conditions concerning bi-Helmholtz operator. Also, this decrease is very significant in the case of higher modes.

- Natural frequencies of the FG nanobeam increase with the rise in porosity volume fraction index and the increase in natural frequencies is more substantial in higher modes.
- The results obtained by both the bi-Helmholtz and Helmholtz operators are almost equal in lower modes. But, in higher modes, the Helmholtz operator possesses more natural frequencies than bi-Helmholtz operator.
- The natural frequencies reduce with the increase in the power-law exponent (k), which means at $k=0$ the beam possesses the highest natural frequencies and at $k=\infty$ the beam retains the lowest natural frequencies.
- The natural frequencies increase with the increase in elastic parameters except for the second mode of CC edge, where some irregularities occur with few combinations for elastic foundations, and these growths are more remarkable with higher modes.

Acknowledgment

The first two authors are very much thankful to Defence Research & Development Organization (DRDO), New Delhi, India (Sanction Code: DG/TM/ERIPR/GIA/17-18/0129/020) for the funding to carry out the present research work.

References

[Ansari et al. 2013] R. Ansari, V. Mohammadi, M. Faghih Shojaei, R. Gholami, and S. Sahmani, "Postbuckling characteristics of nanobeams based on the surface elasticity theory", *Composites Part B: Engineering* **55** (2013), 240-246.

[Ansari et al. 2015] R. Ansari, T. Pourashraf, and R.Gholami, "An exact solution for the nonlinear forced vibration of functionally graded nanobeams in thermal environment based on surface elasticity theory", *Thin-Walled Structures* **93** (2015), 169-176.

[Arefi and Zenkour 2017] M. Arefi, and A. M. Zenkour, "Analysis of wave propagation in a functionally graded nanobeam resting on visco-Pasternak's foundation", *Theoretical and Applied Mechanics Letters* **7** (2017), 145-151.

[Aria and Friswell 2019] A. I. Aria, and M. I. Friswell, "A nonlocal finite element model for buckling and vibration of functionally graded nanobeams", *Composites Part B: Engineering* **166** (2019), 233-246.

[Aydogdu and Taskin 2007] M. Aydogdu, and V. Taskin, "Free vibration analysis of functionally graded beams with simply supported edges", *Materials & design* **28** (2007), 1651-1656.

[Barretta et al. 2018] R. Barretta, F. Fabbrocino, R. Luciano, and F. Marotti de Sciarra, "Closed-form solutions in stress-driven two-phase integral elasticity for bending of functionally graded nano-beams", *Physica E* **97** (2018), 13-30.

[Bay□n and Bayin 2006] □. S. Bay□n, and □. S. Bayin, *Mathematical methods in science and engineering*, John Wiley & Sons, 2006.

[Bekhadda et al. 2019] A. Bekhadda, I. Bensaid, A. Cheikh, and B. Kerboua, "Static buckling and vibration analysis of continuously graded ceramic-metal beams using a refined higher order shear deformation theory", *Multidiscipline Modeling in Materials and Structures*

[Chen et al. 2020] W. R. Chen, C. S. Chen, and H. Chang, "Thermal Buckling Analysis of Functionally Graded Euler-Bernoulli Beams with Temperature-dependent Properties", *Journal of Applied and Computational Mechanics* 6 (2020), 457-70.

[Ebrahimi and Salari 2015] F. Ebrahimi, and E. Salari, "Nonlocal thermo-mechanical vibration analysis of functionally graded nanobeams in thermal environment", *Acta Astronautica* **113** (2015), 29-50.

[Eltaher et al. 2012] M. A. Eltaher, S. A. Emam, and F. F. Mahmoud, "Free vibration analysis of functionally graded size-dependent nanobeams", *Applied Mathematics and Computation* **218** (2012), 7406-7420.

[Eringen 2002] A. C. Eringen, *Nonlocal Continuum Field Theories*, Springer, 2002.

[Esmaeili and Tadi Beni 2019] M. Esmaeili, and Y. Tadi Beni, "Vibration and Buckling Analysis of Functionally Graded Flexoelectric Smart Beam", *Journal of Applied and Computational Mechanics* **5** (2019), 900-17.

[Hadi et al. 2018] A. Hadi, M. Zamani Nejad, and M. Hosseini, "Vibrations of three-dimensionally graded nanobeams", *International Journal of Engineering Science* **128** (2018), 12-23.

[Hamed et al. 2016] M. A. Hamed, M. A. Eltaher, A. M. Sadoun, and K. H. Almitani, "Free vibration of symmetric and sigmoid functionally graded nanobeams", *Applied Physics A* (2016). https://doi.org/10.1007/s00339-016-0324-0

[Hashemi et al. 2014] Sh. Hosseini-Hashemi, R. Nazemnezhad, and M. Bedroud, "Surface effects on nonlinear free vibration of functionally graded nanobeams using nonlocal elasticity", *Applied Mathematical Modelling* **38** (2014), 3538-3553.

[Hosseini and Rahmani 2016] S. A. H. Hosseini, and O. Rahmani, "Thermomechanical vibration of curved functionally graded nanobeam based on nonlocal elasticity", *Journal of Thermal Stresses* **39** (2016), 1252-1267.

[Jena et al. 2019a] S. K. Jena, S. Chakraverty, M. Malikan, and F. Tornabene, "Stability analysis of single-walled carbon nanotubes embedded in winkler foundation placed in a thermal environment considering the surface effect using a new refined beam theory", *Mechanics Based Design of Structures and Machines* (2019). https://doi.org/10.1080/15397734.2019.1698437

[Jena et al. 2019b] S. K. Jena, S. Chakraverty, and M. Malikan, "Implementation of Haar wavelet, higher order Haar wavelet, and differential quadrature methods on buckling response of strain gradient nonlocal beam embedded in an elastic medium", *Engineering with Computers* (2019). https://doi.org/10.1007/s00366-019-00883-1

[Jena et al. 2020a] S. K. Jena, S. Chakraverty, and M. Malikan, "Implementation of non-probabilistic methods for stability analysis of nonlocal beam with structural uncertainties", *Engineering with Computers* (2020). https://doi.org/10.1007/s00366-020-00987-z

[Jena et al. 2020b] S. K. Jena, S. Chakraverty, and M. Malikan, "Vibration and buckling characteristics of nonlocal beam placed in a magnetic field embedded in Winkler–Pasternak elastic foundation using a new refined beam theory: an analytical approach", *The European Physical Journal Plus* (2020). https://doi.org/10.1140/epjp/s13360-020-00176-3

[Jouneghani et al. 2018] F. Zare Jouneghani, R. Dimitri, and F. Tornabene, "Structural response of porous FG nanobeams under hygro-thermo-mechanical loadings", *Composites Part B: Engineering* **152** (2018), 71-78.

[Karami and Janghorban 2019] B. Karami, and M. Janghorban, “A new size-dependent shear deformation theory for free vibration analysis of functionally graded/anisotropic nanobeams”, *Thin-Walled Structures* **143** (2019), 106227.

[Khaniki 2019] H. Bakhshi Khaniki, “On vibrations of FG nanobeams”, *International Journal of Engineering Science* **135** (2019), 23-36.

[Khorshidi and Shariati 2016] M. A. Khorshidi, and M. Shariati, “Free vibration analysis of sigmoid functionally graded nanobeams based on a modified couple stress theory with general shear deformation theory”, *Journal of the Brazilian Society of Mechanical Sciences and Engineering* **38** (2016), 2607–2619.

[Koizumi 1994] M. Koizumi, “The concept of FGM, Ceramic Transactions”, *Functionally Gradient Materials* **34** (1994), 3–10.

[Koutsoumaris and Eptaimeros 2018] C. C. Koutsoumaris, and K. G. Eptaimeros, “A research into bi-Helmholtz type of nonlocal elasticity and a direct approach to Eringen’s nonlocal integral model in a finite body”, *Acta Mechanica* **229**(2018), 3629-3649.

[Lazar et al. 2006] M. Lazar, G. A. Maugin, and E. C. Aifantis, “On a theory of nonlocal elasticity of bi-Helmholtz type and some applications”, *International Journal of Solids and Structures* **43** (2006), 1404-1421.

[Lim et al. 2015] C. W. Lim, G. Zhang, and J. N. Reddy, “A higher-order nonlocal elasticity and strain gradient theory and its applications in wave propagation”, *Journal of the Mechanics and Physics of Solids* **78** (2015), 298-313.

[Malikan 2017] M. Malikan, “Electro-mechanical shear buckling of piezoelectric nanoplate using modified couple stress theory based on simplified first order shear deformation theory”, *Applied Mathematical Modelling* **48** (2017), 196-207.

[Malikan et al. 2020] M. Malikan, M. Krasheninnikov, and V. A. Eremeyev, “Torsional stability capacity of a nano-composite shell based on a nonlocal strain gradient shell model under a three-dimensional magnetic field”, *International Journal of Engineering Science* **148** (2020), 103210.ss

[Mindlin 1965] R. D. Mindlin, “Second gradient of strain and surface-tension in linear elasticity”, *International Journal of Solids and Structures* **1** (1965), 417-438.

[Mirjavadi et al. 2018] S. S. Mirjavadi, B. M. Afshari, M. Khezel, N. Shafiei, S. Rabby, and M. Kordnejad, "Nonlinear vibration and buckling of functionally graded porous nanoscaled beams", *Journal of the Brazilian Society of Mechanical Sciences and Engineering* (2018). https://doi.org/10.1007/s40430-018-1272-8

[Nazemnezhad and Hashemi 2014] R. Nazemnezhad, and Sh. Hosseini-Hashemi, "Nonlocal nonlinear free vibration of functionally graded nanobeams", *Composite Structures* **110** (2014), 192-199.

[Pradhan and Chakraverty 2014] K. K. Pradhan, and S. Chakraverty, "Effects of different shear deformation theories on free vibration of functionally graded beams", *International Journal of Mechanical Sciences* **82** (2014), 149-160.

[Reddy 2007] J. N. Reddy, "Nonlocal theories for bending, buckling and vibration of beams", *International Journal of Engineering Science* **45** (2007), 288-307.

[Saffari et al. 2017] Sh. Saffari, M. Hashemian, and D. Toghraie, "Dynamic stability of functionally graded nanobeam based on nonlocal Timoshenko theory considering surface effects", *Physica B: Condensed Matter* **520** (2017), 97-105.

[Sedighi and Malikan 2020] H. M. Sedighi, and M. Malikan, "Stress-driven nonlocal elasticity for nonlinear vibration characteristics of carbon/boron-nitride hetero-nanotube subject to magneto-thermal environment", *Physica Scripta* **95** (2020), 055218.

[Shafiei et al. 2016] N. Shafiei, M. Kazemi, M. Safi, and M. Ghadiri, "Nonlinear vibration of axially functionally graded non-uniform nanobeams", *International Journal of Engineering Science* **106** (2016), 77-94.

[Shahsavari et al. 2018] D. Shahsavari, M. Shahsavari, L. Li, and B. Karami, "A novel quasi-3D hyperbolic theory for free vibration of FG plates with porosities resting on Winkler/Pasternak/Kerr foundation", *Aerospace Science and Technology* 72 (2018), 134-149.

[Sharabiania and Yazdi 2013] P. A. Sharabiania, and M. R. Haeri Yazdi, "Nonlinear free vibrations of functionally graded nanobeams with surface effects", *Composites Part B: Engineering* **45** (2013), 581-586.

[Simsek 2016] M. Simsek, "Nonlinear free vibration of a functionally graded nanobeam using nonlocal strain gradient theory and a novel Hamiltonian approach", *International Journal of Engineering Science* **105** (2016), 12-27.

[Simsek 2019] M. Simsek, "Some closed-form solutions for static, buckling, free and forced vibration of functionally graded (FG) nanobeams using nonlocal strain gradient theory", *Composite Structures* **224** (2019), 111040.

[Uzun and Yayl□ 2019] B. Uzun, and M. Ö. Yayl□, "Finite Element Model of Functionally Graded Nanobeam for Free Vibration Analysis", *International Journal of Engineering and Applied Sciences* **11**(2019), 387-400.

[Uzun and Yayl□ 2020] B. Uzun, and M.Ö. Yayl□, "Nonlocal vibration analysis of Ti-6Al-4V/ZrO2 functionally graded nanobeam on elastic matrix", *Arabian Journal of Geosciences* **13** (2020), 1-10.

[Vosoughi 2016] A. R. Vosoughi, "Nonlinear Free Vibration of Functionally Graded Nanobeams on Nonlinear Elastic Foundation", *Iranian Journal of Science and Technology, Transactions of Civil Engineering* **40** (2016), 23–32.

[Vu-Bac et al. 2016] N. Vu-Bac, T. Lahmer, X. Zhuang, T. Nguyen-Thoi, and T. Rabczuk, "A software framework for probabilistic sensitivity analysis for computationally expensive models", *Advances in Engineering Software* **100** (2016), 19-31.

[Wattanasakulpong and Ungbhakorn 2014] N Wattanasakulpong, and V Ungbhakorn, "Linear and nonlinear vibration analysis of elastically restrained ends FGM beams with porosities", *Aerospace Science and Technology* **32** (2014), 111-120.

[Zeighampour and Tadi Beni 2015] H. Zeighampour, and Y. Tadi Beni, "Free vibration analysis of axially functionally graded nanobeam with radius varies along the length based on strain gradient theory", *Applied Mathematical Modelling* **39** (2015), 5354-5369.